Computer Methods in Applied Mechanics and Engineering

A coupled multiscale model of the human cornea accounting for the collagenous microstructure and the extracellular matrix

--Manuscript Draft--

Manuscript Number:	CMAME-D-25-02304R1
Article Type:	Research Paper
Keywords:	Cornea; Biological composite; Continuum; Microstructural modeling; Collagen; Crosslinks
Corresponding Author:	Anna Pandolfi Politecnico di Milano Milano, ITALY
First Author:	Christopher Miller
Order of Authors:	Christopher Miller
	Maria Laura De Bellis
	Anna Pandolfi
Abstract:	The cornea is an ocular tissue that forms the clear outermost layer of the eye. Its highly specialized content and organization provide the cornea with mechanical properties that allow it to maintain its spherical shape under the action of intraocular pressure, a factor vital to its function within the eye's refractive system. We propose a coupled multiscale finite element model of the human cornea, where the tissue microstructure is upscaled in terms of a nonlinear trusswork of discrete structural elements, accounting for the stroma's distinctive collagen-crosslink lamellar architecture, and superpose it with continuum solid elements describing the non-collagenous extracellular matrix. As such, the cornea is regarded as a biological composite material with strongly nonlinear properties within a finite kinematics framework. The constitutive description is applied to a patient-specific geometry derived from corneal topography images, model parameters are calibrated to experimental pressure-inflation data, thus providing mechanical behavior representative of the healthy cornea, and the influence of the geometric discretization is also investigated. Most importantly, the presented framework is applied to the evolution of keratoconus, a pathology characterized by the localized protrusion and thinning of the cornea. We demonstrate that the outlined model, despite using relatively simplistic methods, albeit in a novel and innovative way, reproduces the format
Response to Reviewers:	No further comments

Ms. Ref. No.: CMAME-D-25-02304

Title: A coupled multiscale model of the human cornea accounting for the collagenous microstructure and the extracellular matrix

Authors: Christopher Miller, Maria Laura De Bellis, Anna Pandolfi

We thank the reviewers for their thoughtful and accurate review of our manuscript. We've considered all the suggestions that were provided and have made the necessary alterations to the manuscript in order to improve its content and form, hoping to have made it more suitable for CMAME and its audience. In the following discussion, we address each of the reviewers' comments point by point, demonstrating where we have made changes to the manuscript. Blue colour is used to report our thoughts and explanations. Red colour is used to indicate the changes that have been made to improve the manuscript.

Answer to Reviewer #1

"The manuscript presents a finite element model of the human cornea, in which nonlinear truss elements represent collagen fibrils and proteoglycan cross-links, embedded within an incompressible Mooney-Rivlin solid that models the surrounding extracellular matrix. Model parameters are calibrated against ex vivo inflation data, and the framework is applied to simulate keratoconus.

The study addresses a biomechanically interesting problem. The inclusion of parameter calibration, a mesh-dependency analysis, and implementation transparency enhances the overall credibility of the work."

This is a concise and correct description of the content of the manuscript. Thank you.

"However, the computational novelty of the approach remains unclear, and the contribution appears to be primarily incremental. CMAME typically prioritizes methodological innovations in numerical algorithms or computational strategies. In this manuscript, most components appear to be adaptations of standard methods rather than fundamental advances."

We agree with the reviewer that the novelty of the study, which indeed has some conceptual advancements and important methodological innovation, has not been adequately expressed in the original version of the manuscript. We had originally thought that it was sufficiently clear, since we did not find any similar approach (micromechanical structure coupled to continuum in a mesoscale) in the literature relating to soft tissue biomechanics. We are now attempting to convince the reviewer that the work is novel and necessitates the new computational approach presented.

"To clarify and potentially strengthen the computational contribution, I encourage the authors to address the following points:"

1. *"Please clarify how the tangent stiffness derivation in Equations 11-14 differs from classical nonlinear truss formulations, such as those presented in Bonet and Wood (2008) that's already cited in the manuscript".*

We agree with the reviewer that the difference was not sufficiently stressed in the text. We have added the following sentence in Subsection 2.4.1:

The formulation differs from the classical nonlinear truss formulation [Bonet and Wodd: 2008] in that, in addition to being alternatively derived in the material frame, the strain measure employed is the axial stretch of the structural element, ensuring that it is better suited towards characterizing the large deformation of the reinforcing collagenous trusswork.

Additionally, when first introduced within the introduction in Section 1, we mention that it correctly accounts for large deformation

A modified finite element truss formulation is additionally presented, which correctly models the tissue microstructure by accounting for large deformation and material nonlinearity.

2. *"In the proposed dynamic-relaxation solver, what specific performance gains are achieved compared to Newton-Raphson? How does the method scale with increasing mesh size or truss density?"*

We agree with the reviewer that the performance gain of dynamic relaxation versus Newton-Raphson has not been discussed. We have added the following paragraph at the end of Subsection 2.4.3:

It is worth commenting briefly on the choice of the solver. The dynamic relaxation method has been proven to be numerically advantageous in conditions of material softening, as well as in managing contact and self-contact. In such instances, it is superior to other Newton-Raphson based algorithms for two main reasons: (i) it deals easily with strong nonlinearities, since it naturally discriminates between multiple solutions to obtain the stable one, and (ii) and it can be optimally implemented in concurrent computers, as the pseudo-dynamic system of equations reduces to a set of independent equations. Whilst Newton-Raphson requires a small number of expensive iterations (on the order of 10), dynamic relaxation requires many inexpensive iterations (on the order of 1000). Moreover, in terms of scalability regarding the mesh size, for a discretized system with N degrees-of-freedom, standard Newton-Raphson algorithms scale as $O(N^{1.5})$-$O(N^2)$, whereas dynamic relaxation algorithms scale as $O(N)$, thus demonstrating a clear computational advantage when it comes to larger meshes.

3. *"The hybrid discrete-continuum formulation appears to be a straightforward superposition of a truss network onto a solid matrix. Similar embedded approaches (e.g., lattice-in-solid methods) have been previously applied in soft-tissue mechanics. Please clarify what distinguishes your method and what computational advantages it offers over prior work"*

We agree with the reviewer that this point needs to be clarified. We added the following paragraphs within the discussion and conclusions in Section 4.

Numerous studies have utilized a combination of solid elements to model the tissue in focus and structural elements to describe, amongst other things, adjacent tissues, boundary conditions, implants, and medical devices [Erdemir: 2007]. However, there is a scarcity of examples, especially in relation to soft tissue biomechanics, where the underlying material architecture has been explicitly described using conforming structural elements in addition to a solid mesh, each sharing the same degrees of freedom. Curiously, this technique was an early strategy adopted in the modeling of steel rebars within concrete structures [Phillips: 1976], which, barring a few exceptions, such as a recent study on seismic applications [Tanaka: 2016], has since been abandoned because of its inability to characterize cracking and slipping. Concerning biomechanical applications, truss elements representing active muscle fibers and solid elements describing a nonlinear viscoelastic continuum were

combined in the Superpositioned Muscle Finite Element model to capture both active and passive muscle behavior [Hedenstierna: 2008]. In another study, collagen fibers were modeled using a Voronoi-based network within a neo-Hookean matrix to investigate fiber-matrix interaction during uniaxial loading [Lake: 2012]. Along similar lines, discrete 1D fibers were modeled as flexural beams running along the edges of amorphous tetrahedral solid elements [Zhang: 2013]. A somewhat different approach integrated Timoshenko beam elements and a hyperelastic matrix through a mortar-based method, thereby eliminating the need for conforming meshes at the fiber-matrix interface [Kakaletsis: 2023].

Within this broader context, the characteristic organization of the cornea is distinctive, as the entire load-bearing capacity of the tissue is entrusted to the collagen fibril skeleton, which forms a true microstructural scaffold. The presented model, therefore, represents a substantial departure from the aforementioned approaches, which simply embed fibers within the extracellular matrix, typically address the presence of the fibers only in a local sense, and importantly, do not portray constituent fibers as a complex mechanically autonomous structure.

4. *"While the keratoconus case study demonstrates physiological behavior, it is unclear what new computational insight it provides. Are there any sensitivity analyses or predictive advantages relative to existing continuum models?"*

We agree with the reviewer that some clarification is necessary. We added the following paragraph within the discussion and conclusions in Section 4:

The conception of the presented multiscale model was motivated by our long-term goal of effectively modeling the evolution of the keratoconic cornea, which cannot be accurately simulated using traditional continuum models. Specifically, purely continuum models cannot replicate the degree of thinning and the variability in thickness at different locations of the cornea [Pandolfi: 2024]. However, whilst demonstrating a clear improvement in this regard, the model is still unable to suitably capture the thinning of the cornea (50\% based on clinical observations) to the extent that the trusswork alone is able to characterize [Pandolfi: 2023]. It is evident that the progressive degeneration of the microstructure alone does not fully encapsulate keratoconus; it is likely that the deterioration in the content and organization of the corneal stroma is associated with a loss in fluid content, leading to a reduction in volume and therefore thinning. In view of this, enforcement of the incompressibility constraint is not necessarily applicable to the tissue in its diseased state, and a biphasic model of the solid extracellular matrix, currently under development, would be more appropriate in characterizing such phenomena. This work, therefore, represents a fundamental first step, and going forward, the coupling of an explicit microstructure and a poroelastic description of the ECM will be instrumental in modeling the thinning of the cornea in localised regions and in reproducing, according to the specific patient, the actual geometry of the pathology.

5. *"Overall, while the manuscript may be a strong candidate for a biomechanics-oriented journal, in its current form it does not meet the threshold for publication in CMAME. A clearer articulation of the computational innovation, ideally supported by algorithmic or methodological advances beyond standard practices, would improve the manuscript's suitability for reconsideration."*

We agree that a clear articulation of the computational innovation is missing. We added the following sentence within the introduction in Section 1:

This coupled multiscale modeling strategy, where the load-carrying function is provided by an autonomous structural network conforming to a filling continuum matrix, is an innovative approach, not just for the cornea, but for biomechanical applications in general.

and the following paragraphs within the discussion and conclusions in Section 4:

The coupled multiscale model presented in this study is an innovative and versatile framework that explicitly models collagen and crosslink components as distinct structural elements, accounting for the organization of fibrous collagen into a lamellar structure, as well as the spatial arrangement and orientation of fibrils throughout the cornea. To the best of our knowledge, no approach has been applied previously that has upscaled the microstructure in terms of a nonlinear trusswork of discrete fibers, coupled with a solid matrix.

The application of this modeling strategy to the human cornea could provide new insights concerning the relevance of the structural organization on physiological and pathological tissue behaviors, since the progressive loss of stiffness can be attributed to the failure of individual components within the reinforcing microstructure. Similarly, a key advantage is its ability to characterize how different components relate to each other spatially and how this relationship changes with and contributes to the development of disease, for instance, the relative shearing of adjacent collagen lamellae due to a reduction in the density and/or mechanical integrity of crosslinks.

Answer to Reviewer #2

“This paper reports a multiscale computational mechanics model on human cornea. The model is preceded by a very clear overview of the relevant anatomy and structure of the cornea in the context of the eye structure. The original contribution of this work resides in basing the model on the collagen-crosslink architecture as a trusswork of non-linear struts. The model is augmented by the extracellular proteoglycan matrix in terms of finite elasticity. The work is placed in the context of prior research and provides a mechanistic basis for better understanding of pathologies. One correction: in reference [7] change "Survey of Ophthalmogy" to "Survey of Ophthalmology”

We thank the reviewer for their encouraging words and for the attention paid even to the typos.

Answer to Reviewer #3

"The manuscript is interesting and well written. I advise the editor to consider it as a possible publication. Some possible amendments are indicated below, authors may implement them in the way of their own choice"

We thank the reviewer for their kind words, and subsequently list the changes made based on their recommendations

1. *"Pictures and illustrative diagrams are very helpful and high quality. I find it very good to explain the method by relying on such figures. Figure 2 explains the trusses within a brick type element. Does this mean that the truss system (direction of collagen fibrils) does depend on the discretization. If so, then the orientation of the elements are crucial that may be the reason to have such a regular mesh used in this example. It is not a critical point but rather important to clarify in order to prevent readers asking the same question."*

This was already stated in Subsection 2.2, but it was not clear enough. The paragraph has been rewritten in a manner that addresses the concerns of the reviewer:

In furtherance to the discussion of the geometric discretization procedure in the previous section, the mesh is generated in such a way that ensures the orientation of collagen truss elements properly reflects the spatial variation in collagen fibril direction (averaged across the thickness) as observed during the experimental imaging of the cornea [Aghamohammadzadeh: 2004]. Accordingly, the arrangement of the unit cells ensure that the main orientation of the fibrils gradually varies from an orthogonal arrangement at the center, which follows the NT and SI directions, to an orthogonal arrangement at the limbus, where fibrils run circumferentially and radially. Importantly, the regularity of the constructed mesh also ensures that this specific arrangement of the collagen and crosslink truss elements is maintained with increasing degrees of discretization along the principal meridian, N_M. Finally, to ensure an equal number of collagen fibril lamina aligned in the horizontal and vertical directions, the framework is restricted to the consideration of discretized geometries with an odd total number of layers, N_L.

2. *"Figure 2c is also a bit confusing since there are 3 elements in 3D picture but 4 elements on top of each other right next to it. It is possible that a unit cell is different than an element, but the "ECM Solid Finite-Element" indicates that a cubic/brick element is a unit cell as well. If not so, please consider amending the figure or at least caption to prevent a misunderstanding."*

In Figure 2C, there are 3 elements highlighted in the 3D picture of the sectioned mesh, however the diagram right next to it which the reviewer refers to as having 4 unit cells on top of each other, in actuality, only has 3, in accordance with the illustrated sectioned mesh. In order to make the figure clearer to readers, it has been edited to include numbers identifying the layer that the unit cell belongs to, and also nodes have been included in the highlighted part of the sectioned mesh to make it immediately apparent that they're referring to the same number of unit cells. Additionally, the caption has been amended to provide a more thorough explanation of Figure 2C and avoid any potential for confusion:

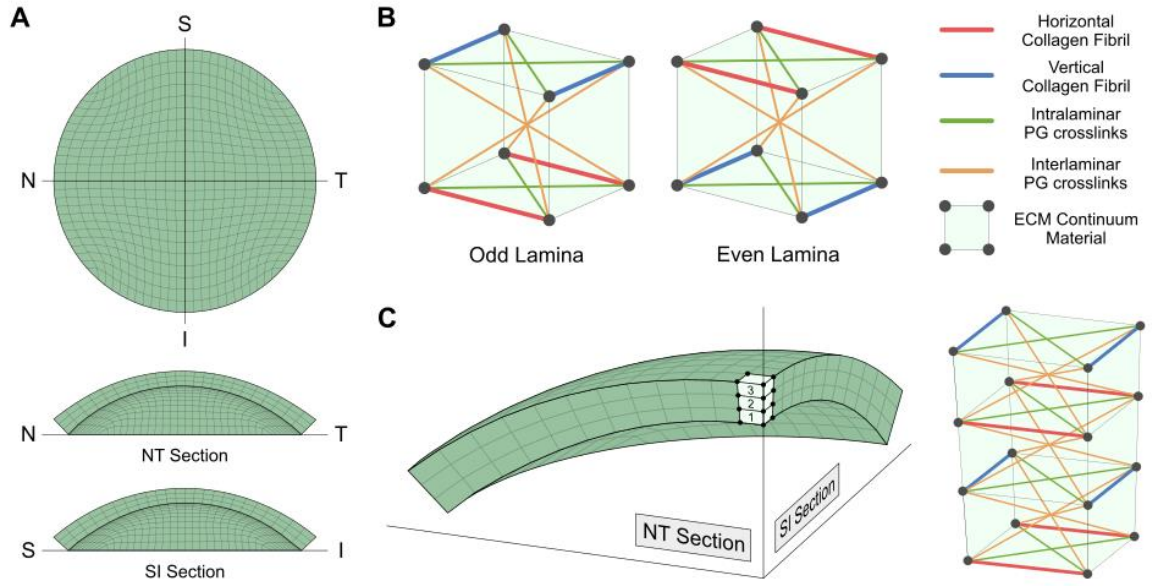

(C) An assembled mesh consisting of three unit cells across the thickness of the corneal geometry (N_L=3), displaying the combined configuration of the three unit cells located at the apex, demonstrating how, over the entire geometry, this will lead to quasi-parallel surfaces of aligned collagen fibrils, (lamina), sequentially alternating in direction.

3. *"Equation (2) is a deformation energy and Eq. (3) is stress derived from it. But the term "stiffness" for Eq. (4) is a bit unclear, normally, we expect an energy or stress definition there as well. Is it stiffness in terms of combining force with stretch or how to understand it? It is later used in Eq. (14) but there it looks like the "stiffness" is in the unit of stress that is quite unusual. By the way, it is neo-Hooke instead of Neo--Hooke, I believe since there were no Mr/s Neo doing the material model."*

The reviewer is correct, this was a mistake so thank you for finding it. We have removed the reference to the stiffness being per unit area, which was obviously wrong, and have instead stated the parameters units. The sentence in Subsection 2.3.1 now reads

(omissis)…where k1 is the elastic stiffness of the fibril (with units of force per area) ...(omissis)

We have also included explicit definitions of the stress and stiffness in equations 3, 4, 6, and 7 to further emphasise where they derive from.

Additionally, Neo-Hookean was altered to neo-Hookean, as per the reviewer's comments.

4. *"Equation (5) introduces a new parameter a that needs to be explained right before or after Eq. (5)."*

Thank you for catching this The first mention of the parameter a in the text now immediately follows Eq. (5) in Subsection 2.3.1:

where ε is the minimum potential energy per unit volume of the crosslink, i.e., the energy in the undeformed state, and a is a non-dimensional parameter.

5. *"Typo: modulous modulus"*

This has been changed, and given that the journal is based in the U.S, we have gone through the manuscript and altered it from British English to American English in its entirety.

6. *"The abbreviations may be repeated in some case, for example, Sect. 2.4.2 is difficult to read with ECM, IOP,... "*

We appreciate the reviewers point of view, and so have gone through the manuscript and removed abbreviations in some areas of the manuscript where it could hinder its readability.

7. *"Figure 3: is unclear if there is data missing that is used for calibration".*

The calibration was included in the manuscript to demonstrate the efficacy of the model, specifically, that it can reliably replicate the pressure-displacement curves for the cornea reported in the literature. The model was fitted to the averaged mechanical response of the data in *[Elsheikh: 2010]*, and so the caption for Figure 3has been altered to explicitly state this:

Calibrated mechanical response of the presented multiscale model for the cornea under the action of the intraocular pressure. The model was fitted to the mean mechanical response of the ex vivo pressure inflation experimental data reported in [elsheikh:2010], for which the range of biological variability is also shown.

8. *"Table 2 shows parameters for shear moduli that may lead to a negative deformation energy that is quite difficult from a numerical perspective to get convergence. It would be beneficial to add a discussion about this issue. By using a stretch larger than 1, authors may have skipped a problem around this issue."*

We thank the reviewer for pointing out this aspect of the model. In our past numerical studies on the cornea, we never reported energy plots, because these are not generally of interest to the ophthalmological community, but we have always verified the positiveness of the global elastic energy of the system. We have added the following paragraph in the comment to Table 2 within Subsection 3.1.

We note that the second stiffness coefficient of the Mooney-Rivlin model, used to describe the extracellular matrix, is negative. In general, this choice must be carefully verified, since it can lead to the global instability of the strain energy. However, since our early work concerning the human cornea, we have made this choice for the characterization of the extracellular matrix, in order to capture the low stiffness of the structure observed at low values of the intraocular pressure [Pandolfi: 2006]. The particular loading conditions (pressurization) and the presence of reinforcing fibers help in avoiding stability issues, and no anomalous behavior has been observed in all our numerical tests.

9. *"I would put Appendix B into the main text since otherwise the dispersion parameter is not well understood in general."*

We thank the reviewer for the comment. We prefer to leave the detailed derivation in the Appendix, since the focus of this study is not the variance model of the two-fiber family

enriched tissue, and this will place too much attention on a pre-existing model. The appendix is only to recall some basic features.

10. *"A general remark is the excessive self citation, it is quite normal that authors make the reader aware of their own works, but the list of publication misses a wider audience by including different groups working in the same topic as well. Here are a few suggestions to look at these works and works citing them in order to increase the list of references in order to decrease the ratio of self citation per others cited. I understand that it is difficult to spot in medical journals mechanicians' contributions, I tried a bit and I am sure that authors can do it even better than me."*

We are sorry, the reviewer is correct, but a significant portion of the literature concerning corneal mechanics has been developed by, or in collaboration with, our research group. We always strive to keep a close eye on parallel works, but we often see the models we develop within the context of our wider body of work. However, we have replaced several of the manuscripts references with analogous works done by other groups in computational ophthalmology; they may not be directly pertinent to this study, but certainly enlarge the landscape of ocular biomechanics.

A coupled multiscale model of the human cornea accounting for the collagenous microstructure and the extracellular matrix

Christopher Miller†, Maria Laura De Bellis[1]†, Anna Pandolfi[2*]†

[1]Department of Engineering and Geology, University of Chieti-Pescara, Viale Pindaro 42, Pescara, 10587, Italy.

[2*]Department of Civil and Environmental Engineering, Politecnico di Milano, Piazza Leonardo da Vinci 32, Milano, 20133, Italy.

*Corresponding author(s). E-mail(s): anna.pandolfi@polimi.it;

†These authors contributed equally to this work.

Abstract

The cornea is an ocular tissue that forms the clear outermost layer of the eye. Its highly specialized content and organization provide the cornea with mechanical properties that allow it to maintain its spherical shape under the action of intraocular pressure, a factor vital to its function within the eye's refractive system. We propose a coupled multiscale finite element model of the human cornea, where the tissue microstructure is upscaled in terms of a nonlinear trusswork of discrete structural elements, accounting for the stroma's distinctive collagen-crosslink lamellar architecture, and superpose it with continuum solid elements describing the non-collagenous extracellular matrix. As such, the cornea is regarded as a biological composite material with strongly nonlinear properties within a finite kinematics framework. The constitutive description is applied to a patient-specific geometry derived from corneal topography images, model parameters are calibrated to experimental pressure-inflation data, thus providing mechanical behavior representative of the healthy cornea, and the influence of the geometric discretization is also investigated. Most importantly, the presented framework is applied to the evolution of keratoconus, a pathology characterized by the localized protrusion and thinning of the cornea. We demonstrate that the outlined model, despite using relatively simplistic methods, albeit in a novel and innovative way, reproduces the formation of a conus to an extent more closely resembling clinical observations than previously reported approaches.

Keywords: Cornea, Biological composite, Continuum, Microstructural modeling, Collagen, Crosslinks

1 Introduction

The cornea is a quasi-spherical transparent shell occupying the outermost part of the eye, that covers the iris, pupil, and anterior chamber, see Fig. 1A. Whilst it serves to protect the eye from infiltrates and ultraviolet radiation, the cornea's primary function is the refraction of light entering the eyeball. It is responsible for approximately two-thirds (43 diopters) of the eye's total optical power [1]. The cornea is made up of several distinct layers through its thickness, each fulfilling a specific role toward the overall functioning of the eye. However, it is the central stroma, making up 90% of the total volume, that dominates the biomechanical properties of the cornea. The stroma consists of a complex architecture of extracellular matrix (ECM) proteins whose specialized structure confers considerable tensile stiffness to the cornea. The tissue is hierarchically organized into numerous (≈300-500) lamellae running parallel to the corneal surface, each of which is composed of aligned bundles of collagen fibrils formed into ribbon-like sheets, with adjacent lamellae arranged at differing angles [2]. Throughout the collagenous microstructure, fibrils are interconnected by proteoglycan (PG) crosslinks which facilitate effective load-transfer and modulate fibril spacing through a careful balance of attractive-repulsive forces [3].

The analysis of the corneal microstructure via X-ray imaging has demonstrated that more than 60% of collagen fibrils have a randomly distributed orientation over the planes tangent to the mid-surface of the cornea, with the remaining 40% exhibiting a more characteristically orthogonal arrangement [4]. In the central cornea, collagen is clearly oriented in the nasal-temporal (NT) and superior-inferior (SI) directions, as a natural response to the activity of the eyelids and eye muscles [5]. Additionally, a prominent circumferential-radial alignment is seen at the periphery of the cornea where it connects with the sclera [6]. The local orthogonality of collagen fibrils is integral to the cornea's ability to sustain a mechanically-stable spherical shape under the action of an intraocular pressure of ≈ 16 mmHg and, critically, ensures the optimal deviation of the light rays onto the retina.

Clinical observations suggest that alterations to the cornea's collagenous architecture are linked to irreversible changes in its spherical geometry, disrupting the proper passage and refraction of light into the eye. A prominent example is keratoconus, a progressive non-inflammatory disorder where a loss in fibril organization leads to the cornea assuming a conical shape and thinning locally [7], see Fig. 1B. This maladaptation can impair a patient's vision considerably, causing symptoms such as irregular astigmatism and high myopia. Additionally, abrupt changes in curvature may result in endothelial rupture, which can severely impact the regulation of the stroma's chemical composition. The etiology of keratoconus and the underlying processes driving its advancement are not fully understood, but its occurrence has been attributed to a range of biological, chemical, genetic, mechanical, and environmental factors [8].

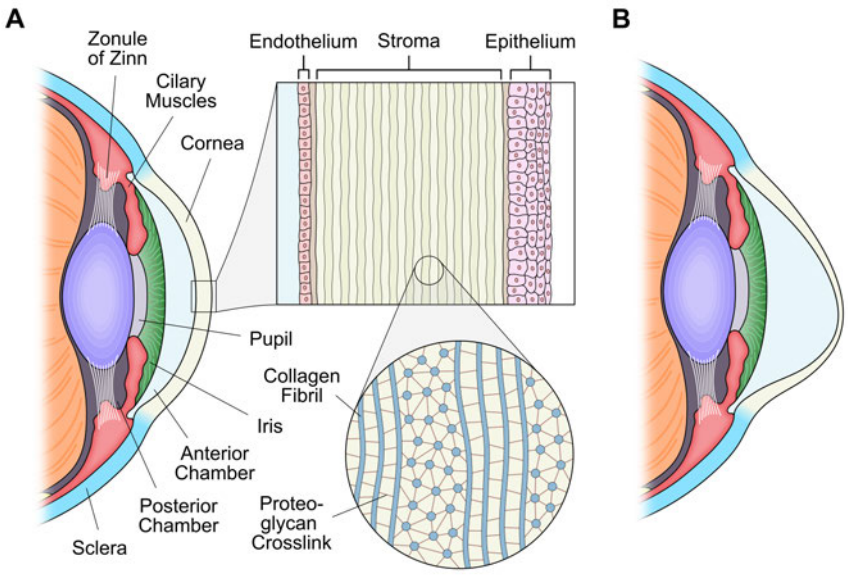

Figure 1 (A) A schematic diagram of the anterior segment of the eye, displaying the repeated structure of the cornea. A magnified view of the stroma demonstrates the organization of the collagenous microstructure into clearly defined lamellae consisting of differentially aligned collagen fibrils interconnected by proteoglycan crosslinks (not to scale). (B) An illustration of the keratoconic cornea, demonstrating the characteristic protrusion and thinning that are hallmark traits of the disease.

Given the many challenges that accompany the experimental assessment of the corneal microstructure, the identification of the deformation mechanisms underpinning healthy functionality and the changes corresponding to a diseased or damaged state are particularly troublesome [9]. Consequently, this has led to the pursuance of computational modeling methods aimed at reproducing the in vivo loading circumstances and replicating the mechanical behavior of the cornea. Beyond their use as a tool to bolster our comprehension of corneal mechanics, they hold great potential toward a host of clinical applications, either in the design and optimization of effective treatment strategies or through their direct introduction within the clinical workflow. Examples include the simulation of contact/contactless testing [10–12], the modeling of refractive surgeries (LASIK, SMILE, etc.) and surgical tools (Keratome, laser, etc.) [13–15], as well as predicting the progression of ectatic disorders such as keratoconus [16–18].

The majority of the numerical studies that have investigated the biomechanical response of the cornea have taken a continuum-based approach. Models of this kind have been employed extensively toward the modeling of numerous soft tissue types, as they can capture fundamental properties such as nonlinearity and anisotropy by accounting for tissue microstructure through a set of reinforcing fibers embedded within a continuum material, as well as other features such as fiber dispersion and spatially varying material stiffness [19–24]. Generally speaking, whilst it is clear that

continuum material descriptions of soft biological tissues can include the influence of mechanically significant proteins and deliver physiologically reasonable outcomes, they often fail to address how specific ECM components relate to each other on a structural basis. They provide a homogenized mechanical response and as such, do not readily integrate information concerning the positioning and combined organization of different constituents [25].

In the context of corneal modeling, continuum models are unable to suitably describe the complex interlinking of collagen fibrils via PG crosslinks, and how their functional interdependency gives rise to macroscopic tissue behavior. The characterization of collagen and crosslink mechanical properties is especially important in the case of models aimed at simulating the evolution of keratoconus, given the association of the pathology with degenerative changes to the collagenous microstructure. Continuum methodologies that have modeled conus formation through tissue weakening resulting from a region-specific temporal reduction of material stiffness have only been able to describe a moderate change in the cornea's spherical shape with limited localized thinning [9, 16]. Models of this kind provide unsatisfactory results as they cannot adequately reflect the loss of structural integrity of the collagen skeleton.

These limitations have prompted the development of microstructurally-motivated discrete models in an effort to provide a more authentic portrayal of the cornea's architecture at sub-macro length scales, whereby the main structural components of the stroma, collagen and PG crosslinks, are explicitly incorporated within a three-dimensional network of structural trusses. The first deployment of this framework modeled all elements as linear elastic and, by simply manipulating the spatial allocation of the stiffness, produced realistic deformation profiles for the healthy and diseased cornea [25]. Subsequent versions examined more histologically appropriate constitutive relations, such as a more realistic pseudo-chemical Lennard-Jones potential to describe crosslink behaviour [26] and a collagen description encompassing the stochastic variation of the orientational dispersion of fibrils [27], with similarly successful outcomes. Other adaptations of the framework have introduced a damage-like scalar field whose evolution is governed by a reaction-diffusion equation [28]. This approach enables a spatial deterioration of element stiffness that can qualitatively predict conus formation.

The collective finding of the aforementioned studies has been the extent to which the weakening of chemical bonds between adjacent lamella heightens transversal shearing and compromises organ-level tissue stability, a feature consistent with experimental observations [7]. The increased deformability of the system leads to localized bulging, pronounced thinning and the reshaping of the cornea, providing a better geometric approximation of keratoconus compared to previous attempts. By directly incorporating key aspects of the microstructure and their impaired mechanical functionality, the various iterations of the outlined discrete modeling framework have demonstrated a substantial improvement in our ability to describe the development of keratoconus.

However, a notable shortcoming of this modeling strategy is that it only considers the reinforcing architecture of the cornea, i.e., it consists solely of struts representing fibrous collagen and associated crosslinks. Neglecting the ECM in which the collagenous microstructure is embedded renders this an incomplete and unrealistic

representation of corneal tissue. Going forward, if the true potential of this simple yet innovative approach is to be fully realized, the presence of the remaining non-collagenous isotropic ECM needs to be appropriately accounted for.

With this in mind, the present work proposes the superposition of the existing discrete microstructural framework with a continuous representation of the non-collagenous matrix, which is modeled as a classical hyperelastic Mooney-Rivlin material. Trusses representing generalized collagen fibrils and PG crosslinks are described by hyperelastic and Lennard-Jones models, respectively. This coupled multiscale modeling strategy, where the load-carrying function is provided by an autonomous structural network conforming to a filling continuum matrix, is an innovative approach, not just for the cornea, but for biomechanical applications in general.A modified finite element truss formulation is additionally presented, which correctly models the tissue microstructure by accounting for large deformation and material nonlinearity. The model is calibrated to provide mechanical behavior representative of the human cornea. The influence of the geometric discretization is investigated, and the ability of the model to characterize keratoconus is compared with previously reported computational models.

The organization of the manuscript is as follows. In Section (2), we introduce the geometry of the cornea, the constitutive models based on microstructural concepts, and the novel aspects of the finite element implementation. Numerical results are collected in Section (3), and a discussion of the proposed model, identifying its significance and potential applications, is reported in Section (4).

2 Materials and methods

2.1 Corneal geometry and microstructure

To arrive at clinically meaningful results, modern advanced computational models of the cornea are built directly from clinical data, whereby patient-specific geometries are constructed through the application of a sophisticated interpolation procedure to a cloud of surface points obtained from corneal topography images [29]. In general, coordinates are in reference to two axes that lie on the vertical plane orthogonal to the optic axis, x corresponding to the NT direction, and y corresponding to the SI direction, with the optic axis taken as the z axis. In the subsequent discussion, we refer to the NT-SI plane as the corneal plane. In this study, the chosen geometry is characterized by a set of shape-related parameters commonly referred to in a clinical setting, which are listed in Table 1.

The geometry is discretized into hexahedral finite elements using an in-house developed 3D grid-generating software, where the discretization process is controlled by two parameters: the number of elements N_M along the principal meridian diameters (NT and SI), and the number of elements N_L across the thickness. An example of a generated mesh is provided in Fig. 2A. The collagenous microstructure, assembled from a series of truss elements, is then superposed onto each solid element to form a unit cell, the configuration of which is detailed in Section (2.2).

The loading of the discretized geometry is provided by imposed tractions (Neumann boundary conditions) associated with the intraocular pressure at the posterior

Table 1 Geometric parameters relating to the anterior and posterior surfaces of the healthy cornea, described as two biconic surfaces. The reference plane contains the x (NT) and y (SI) axes of the model.

	Value	Unit
General		
Central thickness	0.57	mm
Apex elevation	2.48	mm
In-plane diameter	10.60	mm
In-plane orientation		
Steepest meridian NT	0	deg
Flattest meridian SI	90	deg
Anterior surface		
Steepest meridian radius	7.56	mm
Flattest meridian radius	7.41	mm
Asphericity coefficients	1.50	mm
Posterior surface		
Steepest meridian radius	6.47	mm
Flattest meridian radius	6.07	mm
Asphericity coefficients	1.00	mm

surface of the cornea. It is also necessary to impose the displacements (Dirichlet boundary conditions) at the external annulus of the geometry, i.e., the limbus, to properly account for the rotational freedom induced by the relative softness of the neighboring sclera and iris.

It should be noted that the measured geometry of the cornea relates to the tissue in its deformed state under the action of the intraocular pressure. As such, the entirely accurate modeling of the cornea using the finite element method necessitates the recovery of its unstressed configuration. Be that as it may, given the added complexity this would bring to the current study and the fact that our primary motivation is to demonstrate the efficacy and robustness of the presented coupled multiscale model, we simply treat the measured cornea as our referential geometry. This issue will, however, be addressed in future work through the integration of our previously developed inverse stress analysis scheme [16] within the modeling framework.

2.2 Unit cell definition

The microstructure of the cornea is characterized by the spatial repetition of a unit cell, where each unit cell consists of a solid 8-noded hexahedral finite element relating to the non-collagenous ECM material, and a series of truss elements interconnecting the various the nodes of the solid element, representing either a collagen fibril or a PG crosslink.

As illustrated in Fig. 2B, we consider a unit cell to have two possible configurations, corresponding to whether it is located within an odd-numbered or an even-numbered layer, where a layer is defined as a group of unit cells existing at the same depth

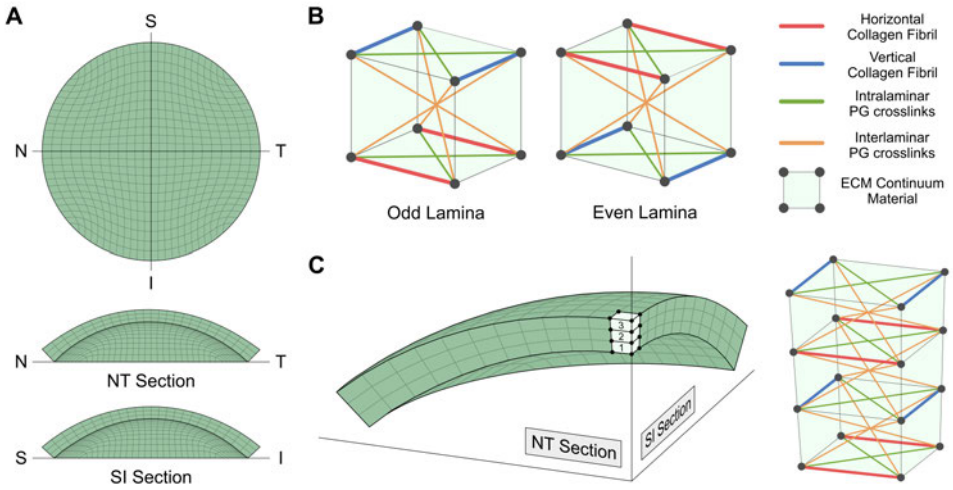

Figure 2 (A) An example of a finite element discretization of the human cornea, consisting of 2,500 nodes and 1,728 8-noded hexahedral elements. (B) The configuration of the unit cell characterizing the generalized microstructure of the cornea, with components describing collagen fibrils, PG crosslinks, and the remaining ECM. The multi-layer assembly of unit cells requires the distinction between those belonging to odd/even layers, so that the ideal organization of the stromal architecture is replicated. (C) An assembled mesh consisting of three unit cells across the thickness of the corneal geometry ($N_L = 3$), displaying the combined configuration of the three unit cells located at the apex, demonstrating how, over the entire geometry, this will lead to quasi-parallel surfaces of aligned collagen fibrils, (lamina), sequentially alternating in direction.

through the thickness of the cornea. The first layer is on the posterior side of the cornea, whilst the number allocated to a layer increases successively in a posterior-to-anterior manner until the maximum is reached on the cornea's anterior side. An odd unit cell contains two vertical collagen trusses interspersed by two horizontal and two diagonal in-plane PG crosslinks located across its top surface, whereas the bottom surface contains two horizontal collagen trusses interspersed by two vertical and two diagonal in-plane PG crosslinks. Finally, four diagonal out-of-plane crosslinks link the nodes of the unit cells' top and bottom surfaces. An even unit cell is then simply the mirror of the odd unit cell in the z-axis. An example assemblage of several unit cells through the thickness of a three-layered discretized geometry is depicted in Fig. 2C. It can be seen that in those instances where multiple adjacent unit cells contain entirely coincident trusses, we model only one truss element that belongs to all neighboring unit cells.

The configuration of unit cells in this way, when assembled to form the corneal geometry in its entirety, gives rise to quasi-parallel surfaces of aligned collagen fibril trusses separated equidistantly throughout the corneal thickness, which we will term laminae. The direction of alignment alternates sequentially in an approximately orthogonal fashion between the horizontal and vertical directions for each successive lamina. Therefore, in accordance with their hypothesized mechanical function, the

in-plane crosslinks act to distance the collagen fibrils within a lamina, whilst the out-of-plane crosslinks effectively separate neighboring laminae. From the arrangement of the PG crosslinks relative to the collagen fibrils, it is readily apparent that their presence will confer the generated trusswork with heightened structural stability compared to if they were absent.

In furtherance to the discussion of the geometric discretization procedure in the previous section, the mesh is generated in such a way that ensures the orientation of collagen truss elements properly reflects the spatial variation in collagen fibril direction (averaged across the thickness) as observed during the experimental imaging of the cornea [6]. Accordingly, the arrangement of the unit cells ensures that the main orientation of the fibrils gradually varies from an orthogonal arrangement at the center, which follows the NT and SI directions, to an orthogonal arrangement at the limbus, where fibrils run circumferentially and radially. Importantly, the regularity of the constructed mesh also ensures that this specific arrangement of the collagen and crosslink truss elements is maintained with increasing degrees of discretization along the principal meridian, N_M. Finally, to ensure an equal number of collagen fibril lamina aligned in the horizontal and vertical directions, the framework is restricted to the consideration of discretized geometries with an odd total number of layers, N_L.

All microstructural-based approaches require a set of assumptions to be made regarding the length-scales reflected in their mathematical framework, and the presented coupled multiscale model is no different. As the wholly realistic portrayal of the tissues' natural micro/nano-scales in a structural sense would require an inordinate number of elements, rendering any simulation far too computationally demanding, the approach taken is to instead assemble a network of trusses representing a more coarse *generalized* form of the collagenous architecture. The individual response of each truss element, in fact, corresponds to a collection of a given constituent. Modeling the hierarchical organization of collagen and PG crosslinks in this way, whilst a simplification compared to the ideal case, still retains our ability to investigate the structure-functional relationship of fibrillar collagen and PG crosslinks and how it imbues corneal tissue with its macroscopic mechanical stiffness and contributes to diseases such as keratoconus.

2.3 Constitutive descriptions

Here we detail the 1D constitutive descriptions of the generalized collagen fibrils and proteoglycan crosslinks, as well as the 3D continuum description accounting for the combined response of the remaining ECM constituents, which are not represented by the assembled trusswork.

2.3.1 Microstructural truss descriptions

The outlined descriptions consider each truss to be a hyperelastic body undergoing large deformations and, thus, employ finite kinematical theory. As such, the relative deformation measure used is the stretch λ, i.e., the deformed length l of the truss, divided by L, its undeformed referential length, where λ is considered to be uniform over the length of the truss. Furthermore, in keeping with experimental observations of

incompressibility concerning fibrous collagen and proteoglycans, we assume all trusses to conserve their volume when deformed.

Given that the traditional treatment of trusses is in a force versus displacement setting, by analogy and for convenience, the formulation is developed in the material reference frame, and therefore, the relations

$$P(\lambda) = \frac{\partial \psi}{\partial \lambda}\,, \quad \mathcal{A}(\lambda) = \frac{\partial P(\lambda)}{\partial \lambda} = \frac{\partial^2 \psi}{\partial \lambda^2}\,, \tag{1}$$

provide the scalar first Piola-Kirchhoff stress P, and the associated scalar stiffness $\mathcal{A}$, of a truss as a function of ψ, its potential energy. It is also worth noting that in the 1D case, P and λ represent an energetic conjugate pairing.

Collagen fibril

The material behavior of a truss representing a generalized collagen fibril is governed by a phenomenological constitutive description, well-established in the literature [30], which accounts for the nonlinear stiffening of soft tissues arising from the recruitment of undulated collagen fibrils. We begin by introducing a quadratic potential energy per unit volume acting along the length of the truss

$$\psi_{\text{coll}}(\lambda) = \frac{k_1}{2k_2}\left[\exp\left\{k_2\left(\lambda-1\right)^2\right\} - 1\right]\,, \tag{2}$$

where k_1 is the elastic stiffness of the fibril (with units of force per area) and k_2 is a dimensionless elastic rigidity parameter. The first Piola-Kirchhoff stress is then defined as

$$P_{\text{coll}}(\lambda) = \frac{\partial \psi_{\text{coll}}(\lambda)}{\partial \lambda} = k_1\left(\lambda-1\right)\exp\left\{k_2\left(\lambda-1\right)^2\right\}\,, \tag{3}$$

which in the absence of the exponential term would reduce to a standard neo-Hookean description. The stiffness is then found to be

$$\mathcal{A}_{\text{coll}}(\lambda) = \frac{\partial^2 \psi_{\text{coll}}(\lambda)}{\partial \lambda^2} = k_1\left[1 + 2k_2\left(\lambda-1\right)^2\right]\exp\left\{k_2\left(\lambda-1\right)^2\right\}\,. \tag{4}$$

which completes our 1D constitutive description for a generalized collagen fibril.

Proteoglycan crosslink

To characterize the mechanical response of the trusses representing the generalized PG crosslinks, we adopt a Lennard-Jones (LJ) potential. LJ models were initially conceived to describe the energy of two interacting objects as a function of the distance between them. They are able to capture the repulsive forces of particles (e.g., atoms, molecules) at close distances, the attractive forces at moderate distances, and the decay of interacting forces at infinite distances.

For this reason, they have also been used to represent the state of equilibrium existing in PG's and the role this plays in modulating the spacing of adjacent collagen

fibrils [26]. Specifically, PG's are prevented from assuming a fully extended conformation, which results in forces that tend to move fibrils closer together. However, PGs are hydrophilic, and the increased water volume leads to forces that push fibrils apart. A careful balance is reached, which in turn gives rise to specific interfibrillar distances.

To phenomenologically describe this behavior, we introduce a potential energy per unit volume of the form

$$\psi_{\mathrm{pg}}(\lambda) = \varepsilon\lambda^{-a}\left(\lambda^{-a} - 2\right) , \tag{5}$$

where ε is the minimum potential energy per unit volume of the crosslink, i.e., the energy in the undeformed state, and a is a non-dimensional parameter. The first Piola-Kirchhoff stress is then denoted by

$$P_{\mathrm{pg}}(\lambda) = \frac{\partial\psi_{\mathrm{pg}}(\lambda)}{\partial\lambda} = 2a\varepsilon\lambda^{-(a+1)}\left(1 - \lambda^{-a}\right) , \tag{6}$$

where it is evident that the parameter, ε, dictates the peak stress of the crosslinks response, whilst a controls the change in stress with increasing axial deformation. The expression

$$\mathcal{A}_{\mathrm{pg}}(\lambda) = \frac{\partial^2\psi_{\mathrm{pg}}(\lambda)}{\partial\lambda^2} = 2\varepsilon a\lambda^{-2(a+1)}\left[2(a+1) - \lambda^a(2+a)\right] , \tag{7}$$

then details the corresponding stiffness and concludes the non-linear constitutive description for a generalized PG crosslink

2.3.2 Continuum extracellular matrix description

The continuum description of the isotropic ECM is determined according to the classical decoupled volumetric-deviatoric formulation of the strain energy density, thus ensuring that incompressibility, a focal feature of corneal tissue, is effectively enforced. The strain energy density is consequently given by

$$\Psi_{\mathrm{ECM}} = \Psi_{\mathrm{vol}}(J) + \Psi_{\mathrm{iso}}(\bar{I}_1, \bar{I}_2) , \tag{8}$$

where Ψ_{vol} denotes a purely volumetric contribution that acts as a penalty term to impose the incompressibility constraint, and Ψ_{iso} is a purely isochoric contribution. The volumetric strain-energy takes the operative form

$$\Psi_{\mathrm{vol}}(J) = \frac{K}{4}(J^2 - 1 - 2\log J) , \tag{9}$$

which depends on the Jacobian $J = \det\mathbf{F}$, where $\mathbf{F} = \partial\mathbf{x}/\partial\mathbf{X}$ is the deformation gradient. The coefficient K is related to the bulk modulus of the material, a suitably high value of which effectively preserves the volume at a Gauss-point [31].

An isotropic hyperelastic Mooney-Rivlin model [32] is assumed for the isochoric part of the deformation, based on its previous successful application to the cornea in

describing the ECM [16]. Accordingly, Ψ_{iso} is defined by the relation

$$\Psi_{\text{iso}}(\bar{I}_1, \bar{I}_2) = \frac{\mu_1}{2}(\bar{I}_1 - 3) + \frac{\mu_2}{2}(\bar{I}_2 - 3)\,, \tag{10}$$

with $\mu = \mu_1 + \mu_2$ denoting the shear modulus of the material, $\bar{I}_1 = \text{tr}(\overline{\mathbf{C}})$ and $\bar{I}_2 = [(\text{tr}(\overline{\mathbf{C}}))^2 - \text{tr}(\overline{\mathbf{C}}^2)]/2$, corresponding to the first and second invariants of the modified right Cauchy-Green deformation tensor, itself described by, $\overline{\mathbf{C}} = \overline{\mathbf{F}}^{\text{T}}\overline{\mathbf{F}}$, where $\overline{\mathbf{F}} = J^{-1/3}\mathbf{F}$ is the modified deformation gradient.

2.4 Finite element formulation

The aspects of the finite element formulation relevant to the present multiscale model of the cornea are briefly recalled. All simulations are carried out using a specifically designed in-house software coded in the programming language C.

2.4.1 Truss elements

We begin by considering a truss element consisting of two nodes $\{\text{a}, \text{b}\}$ whose referential and deformed coordinates are given by the two sets of vectors $\{\mathbf{X}_\text{a}, \mathbf{X}_\text{b}\}$ and $\{\mathbf{x}_\text{a}, \mathbf{x}_\text{b}\}$, respectively. Consequently, the relation $\mathbf{u}_{(\bullet)} = \mathbf{x}_{(\bullet)} - \mathbf{X}_{(\bullet)}$ provides the displacement vector for a given node.

Following on from the constitutive descriptions outlined in Section (2.3.1), the internal forces acting at each node of the truss are denoted by

$$\mathbf{T}_\text{a} = -P(\lambda)A\ \mathbf{n}\,, \quad \mathbf{T}_\text{b} = P(\lambda)A\ \mathbf{n}\,, \tag{11}$$

where A is the referential cross-sectional area, $\mathbf{n} = (\mathbf{x}_\text{b} - \mathbf{x}_\text{a})\,/l$ is a unit vector defining the deformed truss's three-dimensional direction in space, and $P(\lambda)$ is the first Piola-Kirchhoff stress of the truss.

The linearization of the equilibrium equations for each node with respect to the two displacement vectors ultimately yields a set of linear equations for an element, which in matrix representation reads

$$\begin{bmatrix} \mathbf{T}_\text{a} \\ \mathbf{T}_\text{b} \end{bmatrix} = \begin{bmatrix} \mathbf{K}_\text{aa} & \mathbf{K}_\text{ab} \\ \mathbf{K}_\text{ba} & \mathbf{K}_\text{bb} \end{bmatrix} \begin{bmatrix} \mathbf{u}_\text{a} \\ \mathbf{u}_\text{b} \end{bmatrix}. \tag{12}$$

The individual contributions to the element tangent stiffness matrix relate the change in the forces at a node to the change in the current position of a particular node. Each contribution is defined according to the relations

$$\mathbf{K}_\text{aa} = \mathbf{K}_\text{bb} = [\alpha(\lambda) - \beta(\lambda)]\,(\mathbf{n} \otimes \mathbf{n}) + \beta(\lambda)\mathbf{I}\,, \quad \mathbf{K}_\text{ab} = \mathbf{K}_\text{ba} = -\mathbf{K}_\text{aa}\,, \tag{13}$$

where $(\mathbf{n} \otimes \mathbf{n})$ is a second-order unit structural tensor containing the trusses' directional information, and $\mathbf{I}$ denotes the identity tensor. The two terms in Eq. (13a) are analogous to the constitutive and geometric quantities arrived at when deriving the

tangent stiffness matrix for a solid finite element. The deformation-dependent scalars, $\alpha(\lambda)$ and $\beta(\lambda)$, have the units, force per unit length, and are defined by the expressions

$$\alpha(\lambda) = \frac{\mathcal{A}(\lambda)A}{L}\,, \quad \beta(\lambda) = \frac{P(\lambda)A}{l}\,. \tag{14}$$

Their derivation, arising from the directional derivative of the internal truss forces in the material frame, is provided in Appendix A. The formulation differs from the classical non-linear truss formulation [33] in that, in addition to being alternatively derived in the material frame, the strain measure employed is the axial stretch of the structural element, ensuring that it is better suited towards characterizing the large deformation of the reinforcing collagenous trusswork.

As was detailed in Sec. 2.1, all trusses are generalized and thus characterize a collection of a given structural protein. Specifically, the unit cell, the fundamental building block of the corneal model, represents the up-scaling of low-scale microscopic components to the macroscale [34]. Thus, each truss element must account for a certain quantity of the tissue material, which reduces proportionally with the size of the discretization. This can be facilitated in a straightforward way by modifying the referential cross-sectional area A allocated to each element. The internal forces and the tangent stiffness matrix contribution of each truss element are assumed to be a function of both N_M, the number of unit cells along the principal meridian, and N_L, the number of unit cells across the thickness. Thus, the area of all trusses in the assembled meshwork is defined as

$$A = w_M w_L \overline{A} \tag{15}$$

where $w_M = 1/N_M$ and w_L are scalar weighting factors referring to the meridian and thickness discretization, respectively. Note that the collagen and crosslink trusses located entirely (both nodes) on the anterior or posterior surfaces are allocated a weighting of $w_L = 1/2N_L$, whilst the remaining majority of the trusses are allocated a weighting of $w_L = 1/N_L$. As the cross-sectional area carries no explicit physiological meaning, we set the input parameter $\overline{A} = 1$ for all trusses such that the mechanical properties of each truss are then fully encapsulated by their respective constitutive parameters.

2.4.2 Solid elements and boundary conditions

To model the ECM continuum material, we used standard linear 8-noded hexahedral isoparametric elements, whose formulation is well-established in the literature and can be found in standard textbooks, e. g., [35].

The intraocular pressure exerted by the aqueous humor is assumed to act uniformly over the posterior surface of the cornea and to act exclusively on the posterior facets of the solid elements, since the collagen/crosslinks trusses cannot be loaded transversally. The pressure is translated into equivalent nodal forces by using the energetic equivalence that arises from the weak form of the linear momentum balance used in the Galerkin approach. The intraocular pressure acts in the direction normal to the

posterior surface, and as such, the external loading of the system is a function of the cornea's current deformation state and must be recomputed at every time step.

Concerning the displacement boundary conditions at the limbus, previous numerical studies have demonstrated that the dominant mechanical effect of surrounding tissues upon the cornea is that they limit the occurrence of bending moments. We therefore enforce that the cross-section of the cornea at the limbus preserves orthogonality conditions with respect to the deformed mid-section of the shell, reducing the engagement of the tissue in terms of stored energy, an aspect that complies with the concept of energy minimization governing the behavior of biological homeostasis.

2.4.3 Solution methodology

The solution of the quasi-static non-linear problem of the pressurized cornea requires the introduction of a simulation time-frame, $t_n = t_{n-1} + \Delta t$, where Δt is the incremental time step. The finite element spatial discretization of the linear momentum equation leads, following assembly, to a non-linear algebraic system of equations that, at the time t_n, can be written in the form

$$\mathbf{R}_n(\mathbf{u}_n) = \mathbf{T}_n(\mathbf{u}_n) - \mathbf{F}_n \to \mathbf{0}\,, \tag{16}$$

where $\mathbf{T}_n(\mathbf{u}_n)$ is the global internal forces array, $\mathbf{u}_n$ is the global displacement array, and $\mathbf{F}_n = \mathbf{F}_{n-1} + \Delta\mathbf{F}$ is the global external forces array, with the residual array $\mathbf{R}_n(\mathbf{u}_n)$ becoming $\mathbf{0}$ only when equilibrium is satisfied.

In this modeling framework, two solution strategies are implemented, the first of which is the traditional Newton-Raphson method. Linearization of the residual array introduces the tangent stiffness matrix and accompanying set of equations, which read

$$\mathbf{K}_n^k = \frac{\partial \mathbf{R}_n^k}{\partial \mathbf{u}}\,, \quad \mathbf{u}_n^{k+1} = \mathbf{u}_n^k - \left[\mathbf{K}_n^k\right]^{-1} \mathbf{R}_n^k\,,$$

and are solved iteratively at each time point t_n, until global equilibrium, i.e., Eq. (16), is satisfied to a predefined tolerance.

However, given the definition of a unit cell, the proposed multiscale model requires a significant number of elements for even moderately discretized corneal geometries, and the resulting size of the global tangent stiffness matrix can become very large, rendering the simulation cumbersome and computationally expensive. Furthermore, this model was conceived with its application towards the simulation of corneal degeneration in mind. For such problems, progressive tissue softening can potentially lead to accompanying, often severe, numerical issues when using the Newton-Raphson scheme. A more convenient approach is therefore to utilize the dynamic relaxation method [36], where we instead construct a critically damped pseudo-dynamic problem described with a fictitious time $\tilde{t}$ (independent of the timescale of the simulation), defined by the expression

$$\mathbf{R}_n(\mathbf{u}_n) = \mathbf{M}_{\text{fict}}\ddot{\mathbf{u}}_n(\tilde{t}) + \mathbf{D}_{\text{fict}}\dot{\mathbf{u}}_n(\tilde{t}) + \mathbf{T}_n(\mathbf{u}_n, \tilde{t}) - \mathbf{F}_n \to \mathbf{0}\,, \tag{17}$$

and designed for the fastest possible convergence toward the steady-state solution. The internal variables, $\dot{\mathbf{u}}$ and $\ddot{\mathbf{u}}$ are the nodal velocity and acceleration arrays, and $\mathbf{M}_{\text{fict}}$ and $\mathbf{D}_{\text{fict}}$ are the fictitious diagonal mass and damping arrays. The pseudo-dynamic problem in Eq. (17) is numerically integrated with respect to $\tilde{t}$ until the steady-state solution is reached ($\ddot{\mathbf{u}} = \dot{\mathbf{u}} = \mathbf{0}$) and global equilibrium is satisfied to a predefined tolerance.

The pseudo-time $\tilde{t}_k = \tilde{t}_{k-1} + \Delta\tilde{t}$ at each iteration of the dynamic relaxation method is defined by $\Delta\tilde{t}$, an arbitrary chosen pseudo-time step. Since the actual density of the material is not relevant in the static problem, for each solid element the pseudo-time step is used to define an ideal density ρ_e such that the critically stable time step Δt_e, defined by the Courant–Friedrichs–Lewy dynamic stability condition, coincides with the chosen $\Delta\tilde{t}$. For a given element size h_e, the critical Δt_e is defined as

$$\Delta t_e = \frac{h_e}{c_e} \approx h_e \sqrt{\frac{\rho_e}{E_e}} = \Delta\tilde{t} \quad \rightarrow \quad \rho_e = E_e \frac{\Delta\tilde{t}^2}{h_e^2}\,, \tag{18}$$

where c_e is the longitudinal wave speed of the material and E_e is the *average* elastic modulus of the element. The element mass matrix is then obtained via the Galerkin approximation by using the element interpolation functions, row lumped to facilitate the numerical solution.

The damping matrix $\mathbf{D}_{\text{fict}}$ is assumed to scale linearly with $\mathbf{M}_{\text{fict}}$ by a weighting factor $\alpha \approx 2\omega_0$, where ω_0 is the first eigen-frequency of the discretized system, approximated by the stiffness-mass Rayleigh ratio

$$\omega_0{}^2 = \max\left(\frac{\mathbf{du}^{\mathrm{T}}\left[\mathbf{T}_{\mathrm{k}} - \mathbf{T}_{\mathrm{k-1}}\right]}{\mathbf{du}^{\mathrm{T}}\mathbf{M}_{\text{fict}}\mathbf{du}}, 0\right), \tag{19}$$

which has been modified specifically for the dynamic relaxation method [36].

It is worth commenting briefly on the choice of the solver. The dynamic relaxation method has been proven to be numerically advantageous in conditions of material softening, as well as in managing contact and self-contact. In such instances, it is superior to other Newton-Raphson based algorithms for two main reasons: (i) it deals easily with strong nonlinearities, since it naturally discriminates between multiple solutions to obtain the stable one, and (ii) and it can be optimally implemented in concurrent computers, as the pseudo-dynamic system of equations reduces to a set of independent equations. Whilst Newton-Raphson requires a small number of expensive iterations (on the order of 10), dynamic relaxation requires many inexpensive iterations (on the order of 1000). Moreover, in terms of scalability regarding the mesh size, for a discretized system with N degrees-of-freedom, standard Newton-Raphson algorithms scale as $O(N^{1.5}) - O(N^2)$, whereas dynamic relaxation algorithms scale as $O(N)$, thus demonstrating a clear computational advantage when it comes to larger meshes.

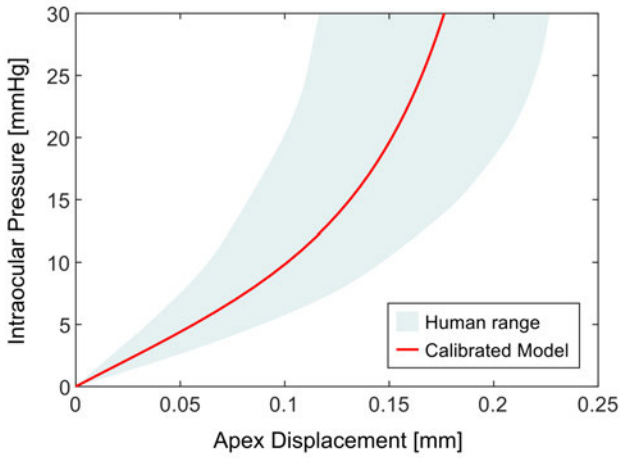

Figure 3 Calibrated mechanical response of the presented multiscale model for the cornea under the action of the intraocular pressure. The model was fitted to the mean mechanical response of the ex vivo pressure inflation experimental data reported in [37], for which the range of biological variability is also shown.

3 Results

3.1 Constitutive parameter calibration

When computationally modeling soft biological tissues, patient-specific geometries can only confer physiologically predictive results by also establishing the corresponding patient-specific material parameters. Unfortunately, in the context of the human cornea, the lack of suitable in vivo mechanical tests that can differentiate the response of the cornea from that of the overall system (eyeball) renders the determination of the tissue's exact constitutive properties a challenging feat. However, to arrive at reasonable numerical results that are realistic to the human cornea, we start by calibrating the proposed multiscale model to experimental data concerning the ex vivo pressure inflation testing of the isolated cornea [37]. The testing protocol implies the complete blockage of the sclera adjacent to the limbus and the progressive increase of the applied intraocular pressure from 0 to 30 mmHg. A corneal geometry with discretization parameters $N_L = 3$ and $N_M = 26$ was used for the fitting. The identified set of constitutive parameters is reported in Table 2, and the mechanical response reached is shown in Fig. 3, demonstrating that the model successfully captures the mean mechanical behavior over the experimental range of variability. The calibrated parameters have been used in the numerical calculations described later.

We note that the second stiffness coefficient of the Mooney-Rivlin model, used to describe the extracellular matrix, is negative. In general, this choice must be carefully verified, since it can lead to the global instability of the strain energy. However, since our early work concerning the human cornea, we have made this choice for the characterization of the extracellular matrix, in order to capture the low stiffness of the

structure observed at low values of the intraocular pressure [16]. The particular loading conditions (pressurization) and the presence of reinforcing fibers help in avoiding stability issues, and no anomalous behavior has been observed in all our numerical tests.

Table 2 Parameters obtained following the calibration of the model to human cornea pressure inflation testing data [37], where discretization parameters of $N_L = 3$ and $N_M = 26$ were used. The table also includes the calibrated parameters for the variance-based model used for comparative analysis [22].

		Value	**Unit**
Coupled multiscale model			
Truss elements			
Referential cross-sectional area	$\overline{A}$	1.00	mm^2
Collagen fibril			
Elastic Stiffness	k_1	1.8	MPa
Rigidity Parameter	k_2	4000	
Proteoglycan crosslink			
Minimum Potential energy	ε	0.01	MPa
Exponent	a	6	
Solid elements			
ECM continuum material			
Shear modulus 1	μ_1	0.0015	MPa
Shear modulus 2	μ_2	-0.0014	MPa
Bulk modulus	K	5	MPa
Variance-based model (two fibril families)			
Solid elements			
Anisotropic collagen-related contribution			
Fibril stiffness parameter (both families)	k_1	0.2	MPa
Fibril rigidity (both families)	k_2	510	
Dispersion coefficient (both families)	κ	location dependent	
Isotropic contribution			
Shear modulus 1	μ_1	0.0015	MPa
Shear modulus 2	μ_2	-0.0014	MPa
Bulk modulus	K	5	MPa

3.2 Influence of the geometric discretization

As the proposed model incorporates a combination of both truss and solid finite elements to upscale the microstructural features of corneal soft tissue to the macroscale, it is necessary to investigate how the geometric discretization impacts the obtained numerical results.

As depicted in Fig. 4A, a unit cell has three dimensions, an out-of-plane height L_{OP}, and two in-plane dimensions. The method of discretization for the corneal geometry ensures that for all the generated unit cells, the two in-plane dimensions are

always approximately equal, and so we use the average in-plane dimension L_{IP} to represent both. A shape factor $f = L_{IP}/L_{OP}$ can then be defined, which provides pertinent information relating to the relative dimensions of a given unit cell, cf. [34]. For instance, a value of $f = 1$ refers to a referential cubic unit cell, whilst values of $f < 1$ and $f > 1$ refer to referential dimensions that are elongated in the out-of-plane and in-plane directions, respectively.

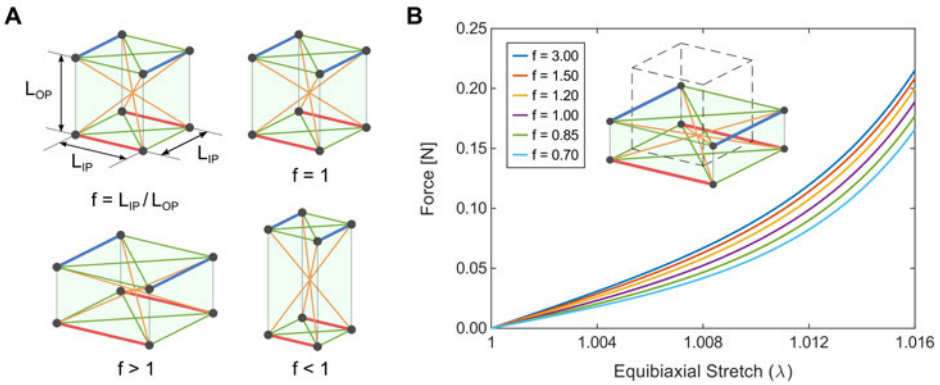

Figure 4 (A) Diagram illustrating the definition of the shape factor f, as well as representative examples of the referential state for the cases of $f = 1$, $f > 1$, and $f < 1$. (B) The mechanical response of a single unit cell exposed to planar equibiaxial tension, for varying values of f, including a diagram showcasing the referential and deformed states for the case of $f = 1$.

The influence of the shape factor f upon the behavior of a single unit cell exposed to planar equibiaxial tension, a loading circumstance closely resembling that of the unit cell in the full organ-level problem, can then be examined. The referential cross-sectional area of the facets over which the force is applied is kept the same for each test to ensure that the continuum ECM force contribution remains the same. From Fig. 4B, it can be seen that for decreasing values of f, the response softens, which is a consequence of the diagonal trusses within the unit cell representing the PG crosslinks. For different values of f, these trusses experience a different axial elongation for the same biaxial deformation of the unit cell, and as such, provide a different contribution to the overall force.

Next, we focus our attention on the effect of the discretization parameters, N_L and N_M, on the mechanical behavior of the pressurized cornea, as the choice of said parameters will obviously dictate the shape of the unit cells that make up the corneal geometry as a whole. This impact is measured through the average value of the shape factor $\bar{f}$ across all resident unit-cells, allowing for an effective comparison of the different degrees of discretization. From Fig. 5A, it can be seen that the influence of the relative dimensions observed for a single unit cell also manifests at the whole organ-level. The number of layers is held constant at $N_L = 3$, whilst the value of N_M is altered. For more elements across the meridian diameter, the magnitude of $\bar{f}$

decreases, and there is a corresponding reduction in the cornea's macroscopic stiffness. From Fig. 5B it is evident that if N_L and N_M are chosen to provide values of $\bar{f}$ that are approximately equal in magnitude, the mechanical behavior of the cornea is relatively consistent, with the minor discrepancies also likely attributable to standard mesh convergence phenomena.

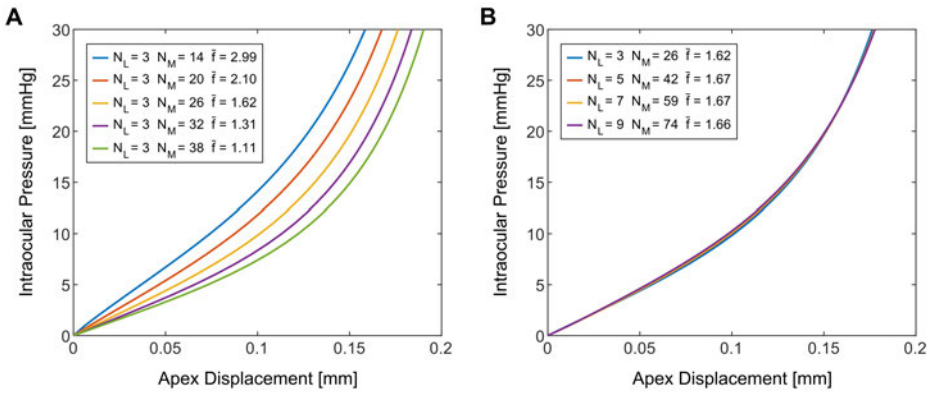

Figure 5 (A) Simulations for differing values of the discretization parameters N_L and N_M that give varying magnitudes of $\bar{f}$ and therefore alternate mechanical behaviors. (B) Simulations for differing values of N_L and N_M that are specifically chosen to give approximately equal magnitudes of $\bar{f}$ and therefore correspondingly equivalent mechanical behavior.

3.3 Application of the model to Keratoconus

The proposed coupled multiscale model has the potential to describe the mechanical outcome of pathologies such as keratoconus, which are characterized by a reduction in material stiffness within a localized area of the cornea, leading to the development of a distinct conical shape. To assess the model's ability to simulate keratoconus, we compare its prediction with that of a phenomenological variance-based continuum model of the corneal stroma, previously applied to the simulation of mechanical tests and refractive surgery procedures [22]. It accounts for the reinforcement of the collagenous matrix via two families of dispersed collagen fibrils, obeying a von Mises orientation distribution governed by a scalar parameter $b(\mathbf{x})$, itself a function of the spatial location within the cornea. The model employs the average and variance of the fourth pseudo-invariant $\overline{I}_4^*$, coupling the orientation of a single fibril to the deformation gradient. As with the coupled multiscale model, we calibrate its material parameters to experimental pressure inflation data (Table 2), such that the mechanical response of both models are approximately equivalent for the healthy eye. Note that both models use the Mooney-Rivlin strain energy function to describe the isotropic ECM material. A brief overview of the variance-based model is provided in Appendix B.

To model the degeneration of the corneal stroma, the various stiffness parameters of both models are reduced according to a scalar damage field $d \in \{0, 1\}$. Clearly, the reduction is not applied to the bulk modulus K, which acts as a penalty coefficient to enforce incompressibility. The spatial distribution of d is assumed to be quadratic and to cover a circular area of radius R = 4 mm, with maximum tissue degeneration ($d = 1$) at the center and no degeneration ($d = 0$) at the boundary of the damaged zone, cf. [27]. The center of the allocated damage field is situated 1 mm towards the inferior side of the cornea, along the SI meridian, in agreement with clinical evidence indicating that keratoconus tends to localize in the lower portion of the corneal surface [7].

The global mechanical response under the action of the intraocular pressure, for the proposed coupled multiscale model and the variance-based model, applied to the healthy and keratoconus cases, is shown in Fig. 6. Whilst the two models predict the same behavior under healthy conditions, they differ for the keratoconus case, with the coupled multiscale model exhibiting greater compliance.

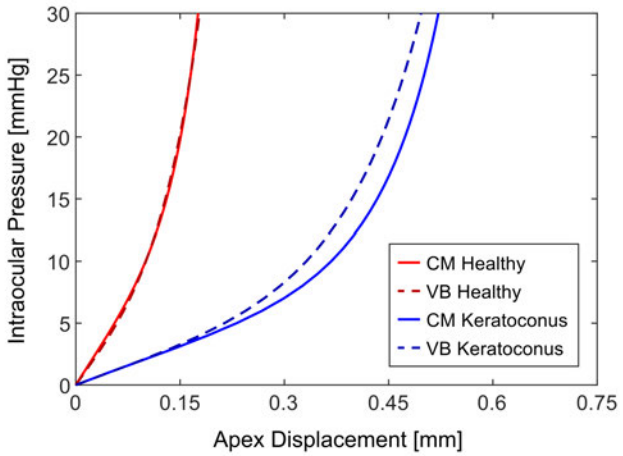

Figure 6 The mechanical response of the presented Coupled multiscale (CM) model and the Variance-based (VB) Model for both the healthy (calibrated to experimental data [37]) and keratoconus case.

SI meridian sections of the cornea are displayed in Fig. 7, demonstrating that both models are able to capture the key features of the pathological configuration. Specifically, Fig. 7A compares the profiles of the healthy and keratoconus corneas obtained with the coupled multiscale model, whilst Fig. 7B compares the same profiles obtained with the variance-based model.

A direct comparison between the keratoconus profiles predicted by the two models is provided in Fig. 7C. The conical protrusion appears slightly more pronounced in the coupled multiscale model, which reveals $\approx 7\%$ higher displacements at the corneal apex. Moreover, a more pronounced thinning is observed in the region of the conus apex, suggesting a more marked stiffness reduction.

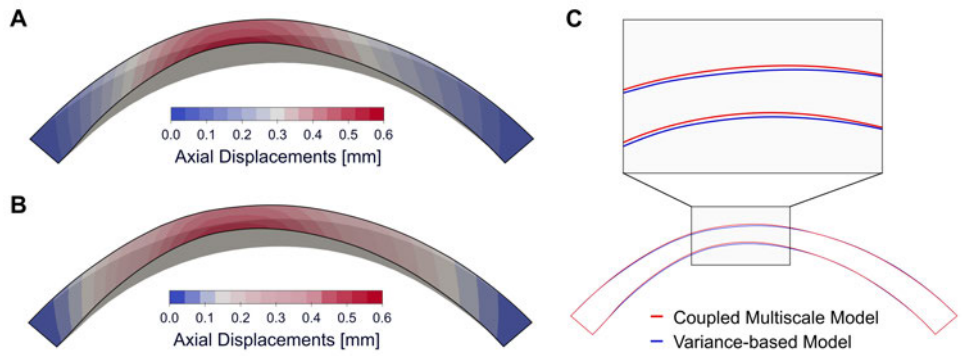

Figure 7 (A) SI meridional profile of the cornea under healthy and keratoconus conditions obtained with the coupled multiscale model. The keratoconus configuration is highlighted with a colour map visualizing the displacements along the optic axis. A conical protrusion has formed, characteristic of keratoconus, with a localized narrowing at the location of maximum damage. (B) SI meridional profile of the cornea under healthy and keratoconus conditions obtained with the variance-based continuum model. Whilst a localized bulging occurs, the deformation is less pronounced than that obtained with the coupled multiscale model. (C) Direct comparison of the SI profile of the keratoconus corneas at physiological intraocular pressure (15 mmHg), obtained with the coupled multiscale and the variance-based models.

4 Discussion and conclusions

In recent times, the computational modeling of biological systems has become a vital tool in supporting the design of surgical and pharmacological treatments. Despite the difficulties associated with the selection of in vivo physical properties, numerical models can, for instance, be used to simulate surgical procedures and augment clinical awareness regarding optimal outcomes, especially when the surgery is risky. They are also becoming increasingly relevant in the study of disease, elucidating the myriad factors linked to the incidence and progression of corneal pathologies. In silico modeling could therefore be the key to solving, or at least partially alleviating, the various mysteries of corneal biomechanics.

Advanced continuum-based numerical models of the human cornea have been successfully deployed in the simulation of healthy physiological states [16], in vivo mechanical tests [10–12], and surgical procedures [13–15]. Nevertheless, such approaches, which often disregard the underlying microstructure, have proven to be insufficient in the modeling of tissue degeneration [9, 16]. Recently, a micromechanical approach upscaled to the organ level has been successfully applied to model the evolution of keratoconus [25, 26]. The approach explicitly accounts for the mechanical interaction of salient features such as fibrous collagen and associated crosslinks by characterizing them as structural truss elements within a spatially repeating unit-cell, which defines the load-carrying lamellar structure of the stroma, thus providing a more physical interpretation of the microstructure compared to entirely phenomenological continuum models.

This study has been devoted to the extension of this existing discrete framework to further include a continuum representation of the non-collagenous ECM in which the mechanically significant constituents are embedded. With the framework now amended to treat the cornea as a solid entity, this multiscale approach now correctly enforces material incompressibility, a hallmark feature of soft biological tissues. It is also well-placed for the possible integration of mathematical descriptions accounting for coupled phenomena such as heat conduction during surgical treatments and fluid/ion fluxes occurring at the posterior surface to preserve corneal transparency. Importantly, the superposition of the collagen trusswork and the ECM continuum within a finite element discretization is computationally straightforward, and the amalgamation of the two approaches has the potential to overcome the fundamental failings of either alone.

The coupled multiscale model presented in this study is an innovative and versatile framework that explicitly models collagen and crosslink components as distinct structural elements, accounting for the organization of fibrous collagen into a lamellar structure, as well as the spatial arrangement and orientation of fibrils throughout the cornea. To the best of our knowledge, no approach has been applied previously that has upscaled the microstructure in terms of a nonlinear trusswork of discrete fibers, coupled with a solid matrix. Numerous studies have utilized a combination of solid elements to model the tissue in focus and structural elements to describe, amongst other things, adjacent tissues, boundary conditions, implants, and medical devices [38]. However, there is a scarcity of examples, especially in relation to soft tissue biomechanics, where the underlying material architecture has been explicitly described using conforming structural elements in addition to a solid mesh, each sharing the same degrees of freedom. Curiously, this technique was an early strategy adopted in the modeling of steel rebars within concrete structures [39], which, barring a few exceptions, such as a recent study on seismic applications [40], has since been abandoned because of its inability to characterize cracking and slipping. Concerning biomechanical applications, truss elements representing active muscle fibers and solid elements describing a nonlinear viscoelastic continuum were combined in the Superpositioned Muscle Finite Element model to capture both active and passive muscle behavior [41]. In another study, collagen fibers were modeled using a Voronoi-based network within a neo-Hookean matrix to investigate fiber-matrix interaction during uniaxial loading [42]. Along similar lines, discrete 1D fibers were modeled as flexural beams running along the edges of amorphous tetrahedral solid elements [43]. A somewhat different approach integrated Timoshenko beam elements and a hyperelastic matrix through a mortar-based method, thereby eliminating the need for conforming meshes at the fiber-matrix interface [44].

Within this broader context, the characteristic organization of the cornea is distinctive, as the entire load-bearing capacity of the tissue is entrusted to the collagen fibril skeleton, which forms a true microstructural scaffold. The presented model, therefore, represents a substantial departure from the aforementioned approaches, which simply embed fibers within the extracellular matrix, typically address the presence of the fibers only in a local sense, and importantly, do not portray constituent fibers as a complex mechanically autonomous structure. The application of this modeling strategy to the human cornea could provide new insights concerning the relevance of

the structural organization on physiological and pathological tissue behaviors, since the progressive loss of stiffness can be attributed to the failure of individual components within the reinforcing microstructure. Similarly, a key advantage is its ability to characterize how different components relate to each other spatially and how this relationship changes with and contributes to the development of disease, for instance, the relative shearing of adjacent collagen lamellae due to a reduction in the density and/or mechanical integrity of crosslinks.

Clearly, a new modeling approach necessitated a revisitation of the material parameters, which have been calibrated to experimental ex vivo data taken from the literature, as well as informed by our past modeling endeavors. An in-depth analysis concerning the effect of the cornea's geometric discretization was also carried out, revealing an inherent mesh-dependency of the model arising from the intra-laminar and inter-laminar crosslinks that form a unit cell. However, most significantly, we have shown that the proposed model, whilst using relatively simplistic numerical methods, albeit in a novel and innovative way, is sufficiently advanced for describing corneal pathologies such as ectasia and keratoconus. By applying a spatial reduction in the stiffness of all tissue constituents, it was possible to simulate localized mechanical instability leading to the formation of a conus to an extent that more closely resembles clinical observations compared to previously reported approaches. Surprisingly, we were also able to obtain favorable results for the variance-based model when applied to the simulation of keratoconus in the cornea, predicting a satisfactory shape for the conus. This can be explained by the fact that, with the support of the couple multiscale model, we have found constitutive parameters somewhat different from those used in previous studies, cf. [28]. Specifically, the proportions of the various mechanical contributions shifted towards a heightened stiffness of the collagen fibrils relative to the isotropic ECM material, following the indications obtained from the coupled multiscale model.

The conception of the presented multiscale model was motivated by our long-term goal of effectively modeling the evolution of the keratoconic cornea, which cannot be accurately simulated using traditional continuum models. Specifically, purely continuum models cannot replicate the degree of thinning and the variability in thickness at different locations of the cornea [28]. However, whilst demonstrating a clear improvement in this regard, the model is still unable to suitably capture the thinning of the cornea (50% based on clinical observations) to the extent that the trusswork alone is able to characterize [26]. It is evident that the progressive degeneration of the microstructure alone does not fully encapsulate keratoconus; it is likely that the deterioration in the content and organization of the corneal stroma is associated with a loss in fluid content, leading to a reduction in volume and therefore thinning. In view of this, enforcement of the incompressibility constraint is not necessarily applicable to the tissue in its diseased state, and a biphasic model of the solid extracellular matrix, currently under development, would be more appropriate in characterizing such phenomena. This work, therefore, represents a fundamental first step, and going forward, the coupling of an explicit microstructure and a poroelastic description of the ECM will be instrumental in modeling the thinning of the cornea in localised regions and in reproducing, according to the specific patient, the actual geometry of the pathology.

There are certain limitations associated with the current model and its implementation. For one, whilst the number of degrees of freedom is unchanged compared to conventional continuum approaches, the large number of truss and solid elements for even moderately discretized geometries can lead to significant computational expense and lengthy simulation times. However, this issue is partially mitigated through concurrent computing, as by using the dynamic relaxation solver, each element is managed independently of the others. Another shortcoming is that the model does not consider the biological and chemical aspects associated with keratoconus and other diseases, such as endothelial dysregulation and corneal swelling. A factor that would be remedied with the inclusion of the previously mentioned biphasic description of the ECM. Lastly, as has already been alluded to, the mathematical portrayal of the microstructure is generalized, representing only a fraction of the lamellae present in the real cornea. Computational limitations at the present time make it infeasible to model the entire collagenous architecture of the cornea in the manner presented here. The behavior of a multilayered trusswork was recently investigated for an increasing number of laminar layers, leading to the definition of a continuum equivalent anisotropic material [34]. Future strategies may also rely on the advent of sophisticated physics-based machine learning techniques to model the lamellar structure and effectively bridge different length-scales.

Finally, the need for patient-specific material properties represents an ongoing challenge if the effective numerical modeling of the cornea for various clinical and research-based applications is to be fully realized, a factor that depends greatly upon the availability of data garnered from in vivo testing methods, which at the present time remains a bottleneck in the modeling of not just the cornea, but all load-bearing soft biological tissues.

Acknowledgements

This work was supported by the Italian Ministry of University and Research (MUR) under the PRIN 2022 project CORTIS (Grant No. 2022TWKA72). AP and MLDB are grateful for the support of the Italian National Group of Physics-Mathematics (GNFM) belonging to the Italian National Institution of High Mathematics "Francesco Severi" (INDAM).

Appendix A Truss Element Tangent Stiffness Matrix Derivation

The derivation of the tangent stiffness matrix relating to a nonlinear large deformation truss element, first introduced during the discussion of the formulation in Section (2.4.1), is a modified form of that presented in [33]. To begin with, the directional derivative of the current length vector, $l\mathbf{n} = (\mathbf{x}_b - \mathbf{x}_a)$, is determined as

$$D\left[\mathbf{x}_b - \mathbf{x}_a\right]\left[\mathbf{u}\right] = \left.\frac{d}{d\epsilon}\right|_{\epsilon=0} \left(\mathbf{x}_b + \epsilon\mathbf{u}_b - \mathbf{x}_a - \epsilon\mathbf{u}_a\right) = \left(\mathbf{u}_b - \mathbf{u}_a\right),$$

which is based on the definitions of the scalar length of the truss, $l = \{(\mathbf{x}_b - \mathbf{x}_a) \cdot (\mathbf{x}_b - \mathbf{x}_a)\}^{1/2}$, and the unit vector, $\mathbf{n} = (\mathbf{x}_b - \mathbf{x}_a)/l$, describing its direction in space. We can then determine the directional derivatives of several quantities required for the subsequent derivation, such as,

$$D\left[l^{-1}(\mathbf{x})\right][\mathbf{u}] = -l^{-2}\mathbf{n} \cdot (\mathbf{u}_b - \mathbf{u}_a)\,,$$

$$D\left[\lambda(\mathbf{x})\right][\mathbf{u}] = \frac{1}{L}\mathbf{n} \cdot (\mathbf{u}_b - \mathbf{u}_a)\,,$$

where, $\lambda = l/L$, is the non-dimensional stretch of the deformed truss. The directional derivative of the truss's internal force at Node b with respect to the elements displacement, $\mathbf{u} = [\mathbf{u}_\mathrm{a}, \mathbf{u}_\mathrm{b}]^T$, following on from the nodal internal force definitions in Eq. (11), and the application of the aforementioned expressions, is then derived as

$$\begin{aligned}
&D\left[\mathbf{T}_b(\lambda(\mathbf{x}), \mathbf{n}(\mathbf{x}))\right][\mathbf{u}] \\
&= D\left[P(\lambda(\mathbf{x}))\right][\mathbf{u}]A\mathbf{n} + P(\lambda)D\left[A\mathbf{n}(\mathbf{x})\right][\mathbf{u}] \\
&= \frac{dP(\lambda)}{d\lambda}D\left[\lambda(\mathbf{x})\right][\mathbf{u}]A\mathbf{n}(\mathbf{x}) + P(\lambda)A\left(D\left[l^{-1}(\mathbf{x})\right][\mathbf{u}](\mathbf{x}_b - \mathbf{x}_a) + \frac{1}{l}D\left[\mathbf{x}_b - \mathbf{x}_a\right][\mathbf{u}]\right) \\
&= \frac{\mathcal{A}(\lambda)A}{L}\mathbf{n} \cdot (\mathbf{u}_b - \mathbf{u}_a)\mathbf{n} + P(\lambda)AlD\left[l^{-1}(\mathbf{x})\right][\mathbf{u}]\mathbf{n} + \frac{P(\lambda)A}{l}(\mathbf{u}_b - \mathbf{u}_a) \\
&= \frac{\mathcal{A}(\lambda)A}{L}\mathbf{n} \cdot (\mathbf{u}_b - \mathbf{u}_a)\mathbf{n} - \frac{P(\lambda)A}{l}\mathbf{n} \cdot (\mathbf{u}_b - \mathbf{u}_a)\mathbf{n} + \frac{P(\lambda)A}{l}(\mathbf{u}_b - \mathbf{u}_a) \\
&= \left(\frac{\mathcal{A}(\lambda)A}{L} - \frac{P(\lambda)A}{l}\right)(\mathbf{n} \otimes \mathbf{n})(\mathbf{u}_b - \mathbf{u}_a) + \frac{P(\lambda)A}{l}(\mathbf{u}_b - \mathbf{u}_a) \\
&= [\alpha(\lambda) - \beta(\lambda)](\mathbf{n} \otimes \mathbf{n})(\mathbf{u}_b - \mathbf{u}_a) + \beta(\lambda)\mathbf{I}(\mathbf{u}_b - \mathbf{u}_a)\,,
\end{aligned}$$

which, given that, $D\left[\mathbf{T}_a(\mathbf{x})\right][\mathbf{u}] = -D\left[\mathbf{T}_b(\mathbf{x})\right][\mathbf{u}]$, due to Eq. (11), gives rise to the matrix representation of the element tangent stiffness matrix detailed in Eq. (12) with the individual contributions provided in Eq. (13).

Appendix B Variance-based continuum model of corneal tissue

A brief overview of the key aspects relating to the variance-based model is provided here; however, for a more expansive detailing, the reader is referred to [22]. The model consists of two families of spatially dispersed collagen fibrils, such that the cornea is represented as a reinforced anisotropic material, where the specific orientation of

fibrils follows the most advanced findings in the literature [6]. The total strain energy consists of three terms

$$\Psi = \Psi_{\text{vol}} + \Psi_{\text{iso}} + \Psi_{\text{aniso}}\,,$$

with Ψ_{vol} denoting the volumetric strain energy, which takes the form

$$\Psi_{\text{vol}}(J) = \frac{1}{4}\,K\,(J^2 - 1 - 2\log J),$$

where $J > 0$ is the determinant of the deformation gradient $\mathbf{F}$, and K a penalization coefficient analogous to the bulk modulus. The isotropic energy Ψ_{iso} follows the Mooney-Rivlin model and is defined as

$$\Psi_{\text{iso}}(\overline{I}_1, \overline{I}_2) = \frac{1}{2}\mu_1(\overline{I}_1 - 3) + \frac{1}{2}\mu_2(\overline{I}_2 - 3)\,, \quad \overline{I}_1 = \operatorname{tr}\overline{\mathbf{C}}\,, \quad \overline{I}_2 = \frac{1}{2}[(\operatorname{tr}\overline{\mathbf{C}})^2 - \operatorname{tr}(\overline{\mathbf{C}}^2)]\,,$$

where $\mu = \mu_1 + \mu_2$ is the elastic shear modulus of the material. The terms $\overline{I}_1$ and $\overline{I}_2$ denote the first and the second invariants, respectively, of the isochoric Cauchy-Green deformation tensor $\overline{\mathbf{C}} = \overline{\mathbf{F}}^T\overline{\mathbf{F}}$, with $\overline{\mathbf{F}} = J^{-1/3}\mathbf{F}$. The anisotropic strain energy Ψ_{aniso} describing the contribution of the two collagen fibril families is

$$\Psi_{\text{aniso}}(\overline{I}^*_{4M}, \sigma^2_{I_4 M}) = \sum_{M=1}^{2} \frac{k_{1M}}{2k_{2M}} \exp\left[k_{2M}\left(\overline{I}^*_{4M} - 1\right)^2\right]\left(1 + K^*_M(\overline{I}^*_{4M})\sigma^2_{I_4 M}\right),$$

where k_{1M} is a stiffness parameter, controlling the fibril behavior at moderate deformations, and k_{2M} is a dimensionless rigidity parameter, regulating the response at large deformations. The pseudo-invariants $\overline{I}^*_{4M}$ are defined as

$$\overline{I}^*_{4M} = \mathbf{H}_M : \overline{\mathbf{C}}\,, \quad \mathbf{H}_M = \langle \mathbf{A}_M \otimes \mathbf{A}_M \rangle = \kappa_M \mathbf{I} + (1 - 3\kappa_M)\mathbf{A}_{M0}\,, \quad \mathbf{A}_M = \mathbf{a}_M \otimes \mathbf{a}_M\,,$$

where $\langle \bullet \rangle$ denotes the average over the unit sphere, $\mathbf{A}_{M0} = \mathbf{a}_0 \otimes \mathbf{a}_0$ refers to the main orientation of the fibril distribution, and the scalar parameter κ_M is defined according to

$$\kappa_M = \frac{1}{4}\int_0^\pi \rho_M(\Theta)\sin^3\Theta d\Theta\,,$$

where $\rho_M(\Theta)$ is the spatial probability distribution (e.g., von Mises). Finally, the relations

$$\sigma^2_{I_4 M} = \overline{\mathbf{C}} : \langle \mathbf{A}_M \otimes \mathbf{A}_M \rangle : \overline{\mathbf{C}} - \left(\mathbf{H}_M : \overline{\mathbf{C}}\right)^2, \quad K^*_M(\overline{I}^*_{4M}) = k_{2M} + 2\,k^2_{2M}\,\left(\overline{I}^*_{4M} - 1\right)^2$$

provide the variance contribution to Ψ_{aniso} and its amplification coefficient, respectively.

References

[1] Mishima, S., Hedbys, B.O.: Physiology of the cornea. International ophthalmology clinics **8**(3), 527–560 (1968)

[2] Bron, A.J.: The architecture of the corneal stroma. British Journal of Ophthalmology **85**, 379–383 (2001)

[3] Maurice, D.M.: The structure and transparency of the cornea. The Journal of physiology **136**(2), 263 (1957)

[4] Abahussin, M., Hayes, S., Cartwright, N.E.K., Kamma-Lorger, C.S., Khan, Y., Marshall, J., Meek, K.M.: 3D collagen orientation study of the human cornea using X-ray diffraction and femtosecond laser technology. Investigative Ophthalmology & Visual Science **50**(11), 5159–5164 (2009) https://doi.org/10.1167/iovs.09-3669

[5] Meek, K.M., Blamires, T., Elliot, G.F., Gyi, T.J., Nave, C.: The organization of collagen fibrils in the human corneal stroma: a synchroton x-ray diffraction study. Current Eye Research **6**, 841–846 (1987)

[6] Aghamohammadzadeh, H., Newton, R.H., Meek, K.M.: X-ray scattering used to map the preferred collagen orientation in the human cornea and limbus. Structure **12**(2), 249–256 (2004)

[7] Rabinowitz, Y.S.: Keratoconus. Survey of Ophthalmology **42**, 297–319 (1998)

[8] Santodomingo-Rubido, J., Carracedo, G., Suzaki, A., Villa-Collar, C., Vincent, S.J., S., W.J.: Keratoconus: An updated review. Contact Lens and Anterior Eye **45**(3), 101559 (2022) https://doi.org/10.1016/j.clae.2021.101559

[9] Simonini, I., Ni Annaidh, A., Pandolfi, A.: Numerical estimation of stress and refractive power maps in healthy and keratoconus eyes. Journal of the Mechanical Behavior of Biomedical Materials **131**, 105252 (2022)

[10] Ariza-Gracia, M.A., Zurita, J.F., Piñero, D.P., Rodriguez-Matas, J.F., Calvo, B.: Coupled biomechanical response of the cornea assessed by non-contact tonometry. A simulation study. PLoS ONE **10**(3), 0121486 (2015)

[11] Simonini, I., Pandolfi, A.: The influence of intraocular pressure and air jet pressure on corneal contactless tonometry tests. Journal of the Mechanical Behavior of Medical Biomaterials **58**, 75–89 (2016) https://doi.org/10.1016/j.jmbbm.2015.07.030

[12] Redaelli, E., Calvo, B., Rodriguez Matas, J.F., Luraghi, G., Grasa, J.: Non-contact tonometry: predicting intraocular pressure using a material—corneal

thickness—independent methodology. Frontiers in Bioengineering and Biotechnology **Volume 12 - 2024** (2024) https://doi.org/10.3389/fbioe.2024.1406870

[13] Studer, H.P., Riedwyl, H., Amstutz, C.A., Hanson, J.V.M., Büchler, P.: Patient-specific finite-element simulation of the human cornea: A clinical validation study on cataract surgery. Journal of Biomechanics **46**(4), 751–758 (2013) https://doi.org/10.1016/j.jbiomech.2012.11.018

[14] Ariza-Gracia, M.A., Ortillés, , Cristóbal, J., Rodriguez-Matas, J.F., Calvo, B.: A numerical-experimental protocol to characterize corneal tissue with an application to predict astigmatic keratotomy surgery. Journal of the Mechanical Behavior of Biomedical Materials **74**, 304–314 (2017) https://doi.org/10.1016/j.jmbbm.2017.06.017

[15] Montanino, A., Overbeeke, S., Pandolfi, A.: Modeling the biomechanics of laser corneal refractive surgery. Journal of the Mechanical Behavior of Biomedical Materials **145**, 105998 (2023)

[16] Pandolfi, A., Manganiello, F.: A material model for the human cornea. constitutive behavior and numerical analysis. Biomechanics and Modelling in Mechanobiology **5**, 237–246 (2006)

[17] Fantaci, B., Calvo, B., Rodriguez Matas, J.F.: Modeling biological growth of human keratoconus: On the effect of tissue degradation, location and size. Computers in Biology and Medicine **180**, 108976 (2024) https://doi.org/10.1016/j.compbiomed.2024.108976

[18] Falgayrettes, N., Patoor, E., Cleymand, F., Zevering, Y., Perone, J.M.: Biomechanics of keratoconus: Two numerical studies. PLOS ONE **18**(2), 1–25 (2023) https://doi.org/10.1371/journal.pone.0278455

[19] Studer, H., Larrea, X., Riedwyl, H., Büchler, P.: Biomechanical model of human cornea based on stromal microstructure. Journal of Biomechanics **43**(5), 836–842 (2010) https://doi.org/10.1016/j.jbiomech.2009.11.021

[20] Whitford, C., Studer, H., Boote, C., Meek, K.M., Elsheikh, A.: Biomechanical model of the human cornea: Considering shear stiffness and regional variation of collagen anisotropy and density. Journal of the Mechanical Behavior of Medical Biomaterials **42**, 76–87 (2015) https://doi.org/10.1016/j.jmbbm.2014.11.006

[21] Nambiar, M., Seiler, T.G., Büchler, P.: Depth-dependent, experimental characterization of the human corneal stroma. Investigative Ophthalmology & Visual Science **64**(8), 1685–1685 (2023)

[22] Pandolfi, A., Vasta, M.: Fiber distributed hyperelastic modeling of biological tissues. Mechanics of Materials **44**, 151–162 (2012)

[23] Miller, C., Gasser, T.C.: A microstructurally motivated constitutive description of collagenous soft biological tissue towards the description of their non-linear and time-dependent properties. Journal of the Mechanics and Physics of Solids **154**, 104500 (2021) https://doi.org/10.1016/j.jmps.2021.104500

[24] Miller, C., Gasser, T.C.: A bottom-up approach to model collagen fiber damage and failure in soft biological tissues. Journal of the Mechanics and Physics of Solids **169**, 105086 (2022) https://doi.org/10.1016/j.jmps.2022.105086

[25] Pandolfi, A., Gizzi, A., Vasta, M.: A microstructural model of cross-link interaction between collagen fibrils in the human cornea. Philosophical Transactions of the Royal Society A **377**(2144), 20180079 (2019)

[26] Pandolfi, A., De Bellis, M.L., Gizzi, A., Vasta, M.: Modeling the degeneration of the collagen architecture in a microstructural model of the human cornea. Mathematics and Mechanics of Solids **28**(1), 196–207 (2023)

[27] De Bellis, M.L., Vasta, M., Gizzi, A., Pandolfi, A.: A numerical model of the human cornea accounting for the fiber-distributed collagen microstructure. Mathematics and Mechanics of Solids, 10812865231202024 (2023)

[28] Pandolfi, A., De Bellis, M.L.: Continuum versus micromechanical modeling of corneal biomechanics. Mechanics of Materials **199**, 105162 (2024)

[29] Simonini, I., Pandolfi, A.: Customized finite element modelling of the human cornea. PloS one **10**(6), 0130426 (2015)

[30] Holzapfel, G.A., Gasser, T.C., Ogden, R.W.: A new constitutive framework for arterial wall mechanics and a comparative study of material models. Journal of Elasticity **61**, 1–48 (2000)

[31] Simo, J.C., Taylor, R.L.: Quasi-incompressible finite elasticity in principal stretches. continuum basis and numerical algorithms. Computer Methods in Applied Mechanics and Engineering **85**(3), 273–310 (1991) https://doi.org/10.1016/0045-7825(91)90100-K

[32] Rivlin, R.S., Saunders, D.W.: Large elastic deformations of isotropic materials. VII. Experiments on the deformation of rubber. Phylosophycal Transactions of The Royal Society of London, A **243** (1951)

[33] Bonet, J., Wood, R.D.: Nonlinear Continuum Mechanics for Finite Element Analysis, 2nd edn. Cambridge University Press, Cambridge (2008)

[34] Köry, J., Stewart, P.S., Hill, N.A., Luo, X.-Y., Pandolfi, A.: A discrete-to-continuum model for the human cornea with application to keratoconus. Royal Society Open Science **11**(7), 240265 (2024)

[35] Belytschko, T., Liu, W.-K., Moran, B., Elkhodary, K.: Nonlinear Finite Elements for Continua and Structures. John Wiley & Sons, New Jersey (2014)

[36] Oakley, D.R., Knight Jr, N.F.: Adaptive dynamic relaxation algorithm for non-linear hyperelastic structures part i. formulation. Computer methods in applied mechanics and engineering **126**(1-2), 67–89 (1995)

[37] Elsheikh, A.: Finite element modeling of corneal biomechanical behavior. Journal of Refractive Surgery **26**(4), 289–300 (2010)

[38] Erdemir, A., McLean, S., Herzog, W., Bogert, A.J.: Model-based estimation of muscle forces exerted during movements. Clinical Biomechanics **22**(2), 131–154 (2007) https://doi.org/10.1016/j.clinbiomech.2006.08.003

[39] Phillips, D.V., Zienkiewicz, O.C.: Finite element non-linear analysis of concrete structures. Proceedings of the Institute of Civil Engineering of London **61**(pt 2), 59–88 (1976) https://doi.org/10.1680/iicep.1976.3503

[40] Tanaka, S., Hori, M., Ichimura, T.: Hybrid finite element modeling for seismic structural response analysis of a reinforced concrete structure. Journal of earthquake and tsunami **10**(05), 1640015 (2016)

[41] Hedenstierna, S., Halldin, P., Brolin, K.: Evaluation of a combination of continuum and truss finite elements in a model of passive and active muscle tissue. Computer Methods in Biomechanics and Biomedical Engineering **11**(6), 627–639 (2008) https://doi.org/10.1080/17474230802312516

[42] Lake, S.P., Hadi, M.F., Lai, V.K., Barocas, V.H.: Mechanics of a fiber network within a non-fibrillar matrix: model and comparison with collagen-agarose co-gels. Annals of Biomedical Engineering **40**, 2111–2121 (2012)

[43] Zhang, L., Lake, S.P., Barocas, V.H., Shephard, M.S., Picu, R.C.: Cross-linked fiber network embedded in an elastic matrix. Soft Matter **9**(28), 6398–6405 (2013)

[44] Kakaletsis, S., Lejeune, E., Rausch, M.: The mechanics of embedded fiber networks. Journal of the Mechanics and Physics of Solids **181**, 105456 (2023) https://doi.org/10.1016/j.jmps.2023.105456

Figure 1

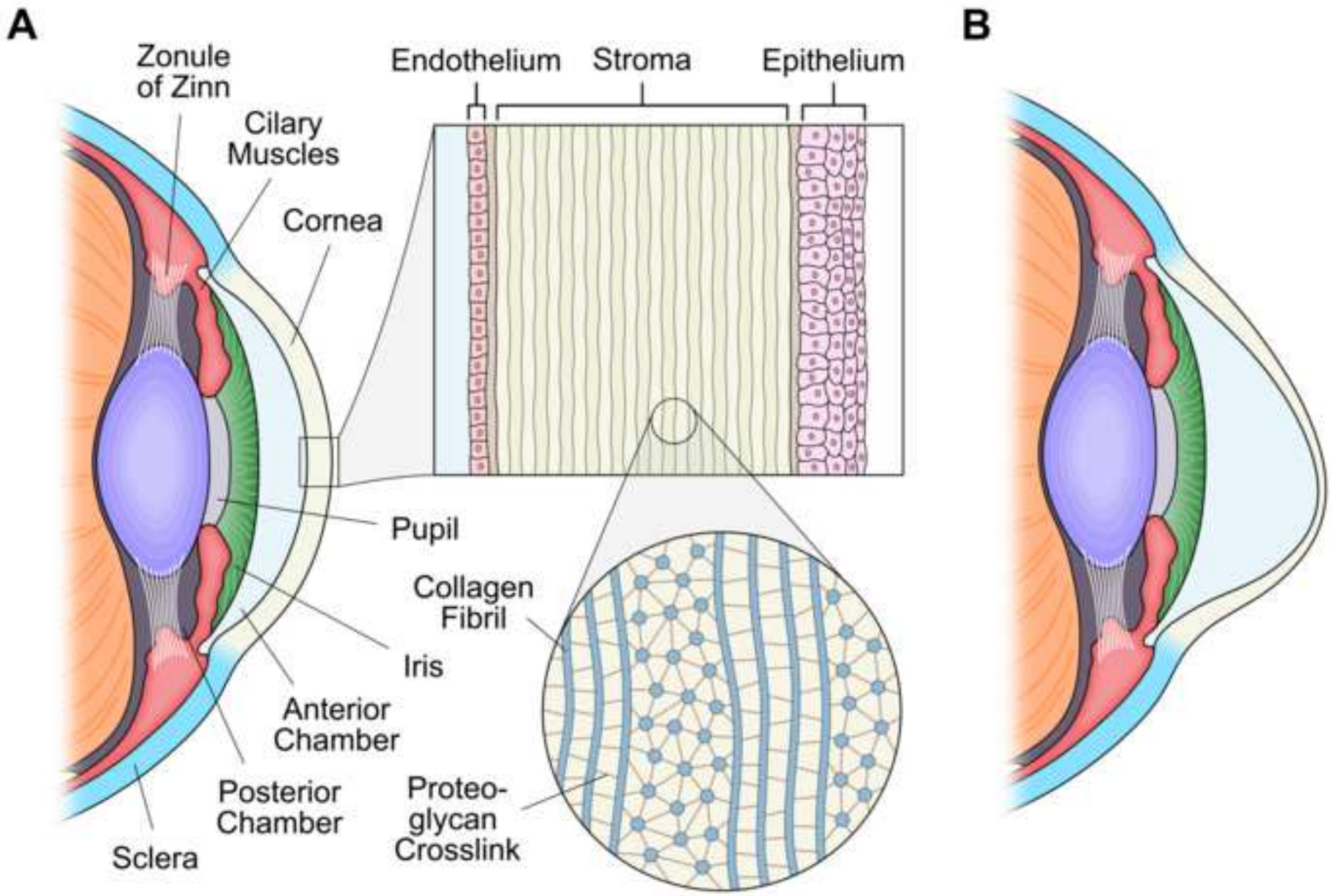

Figure 2

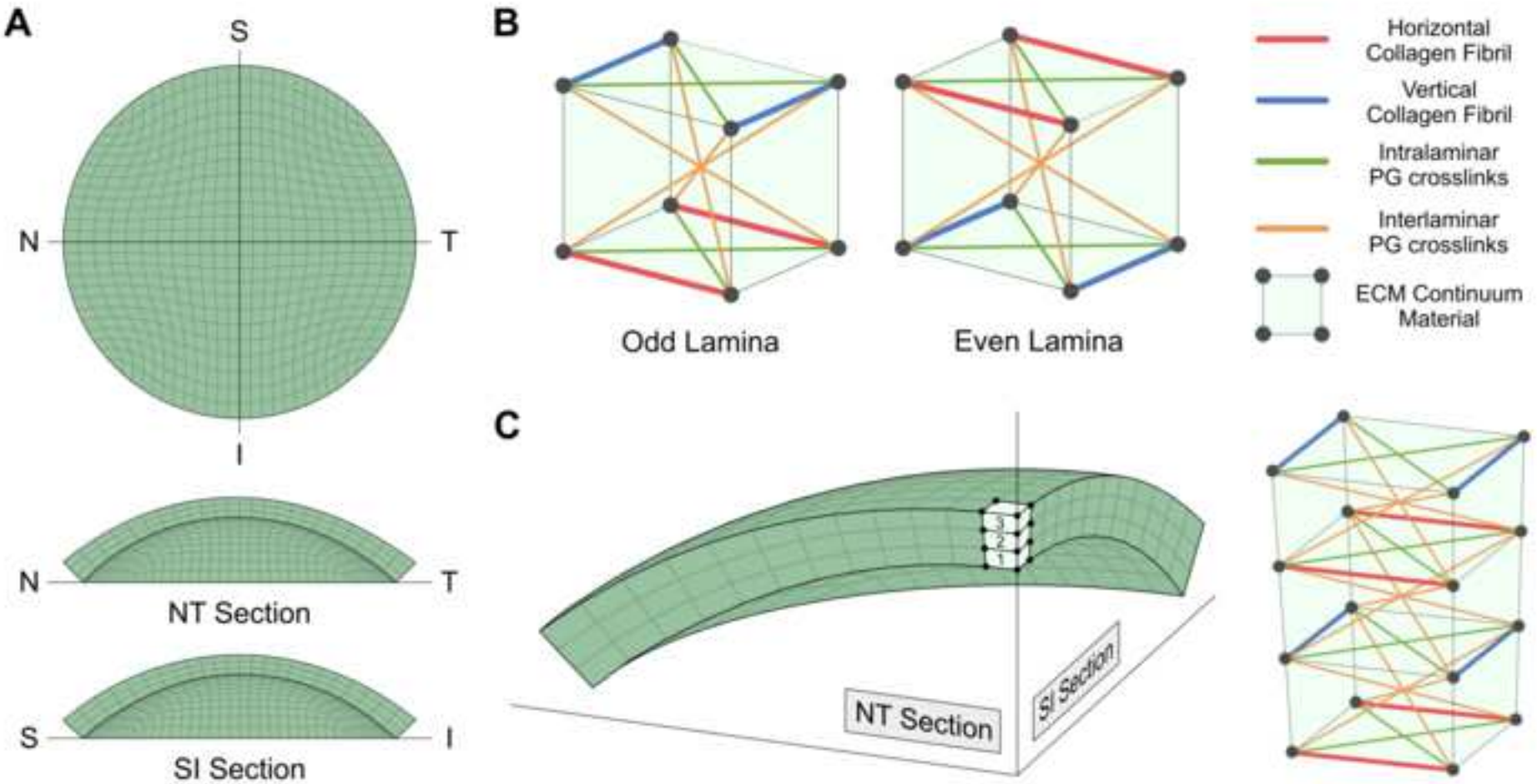

Figure 3

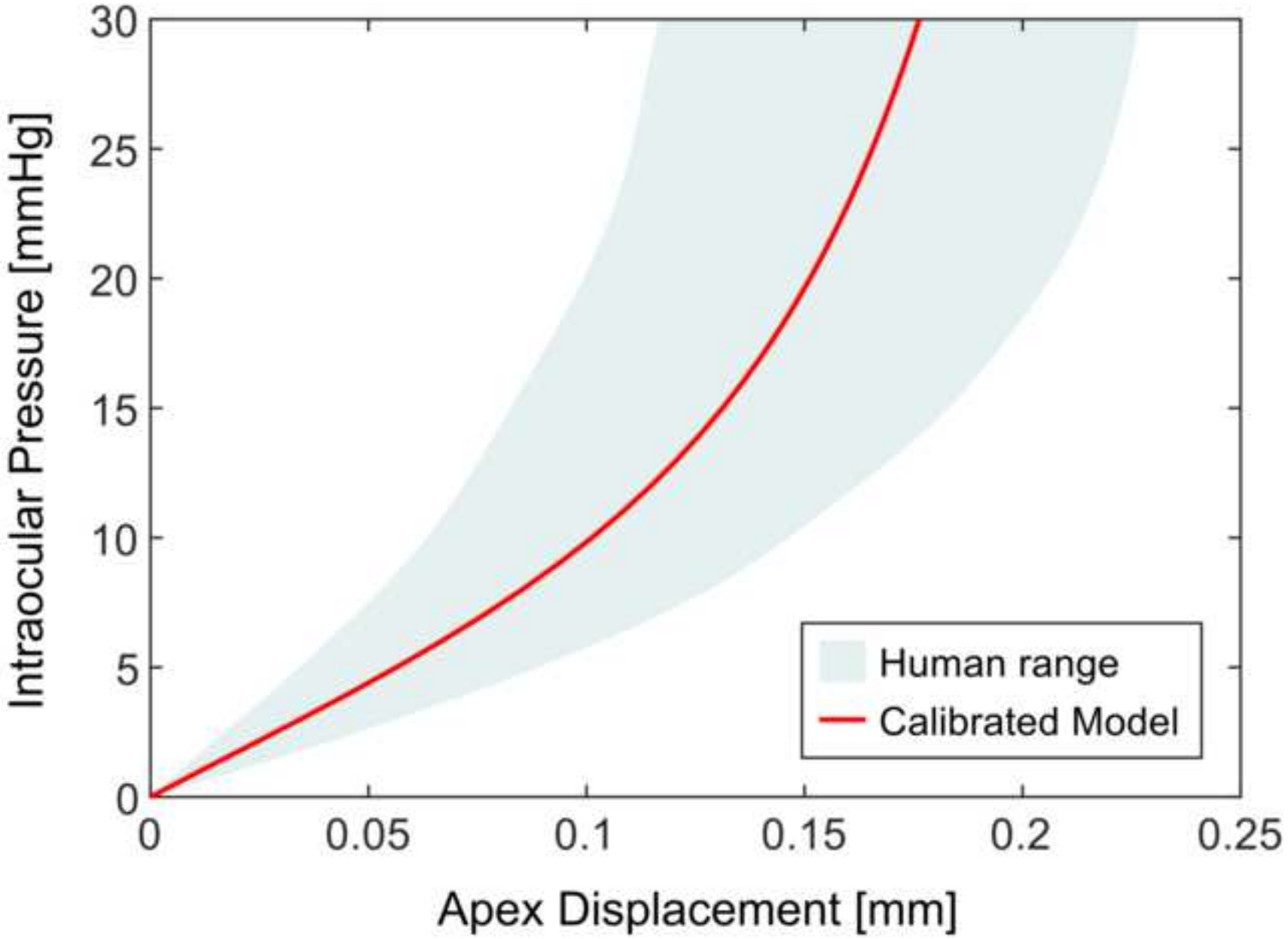

Figure 4

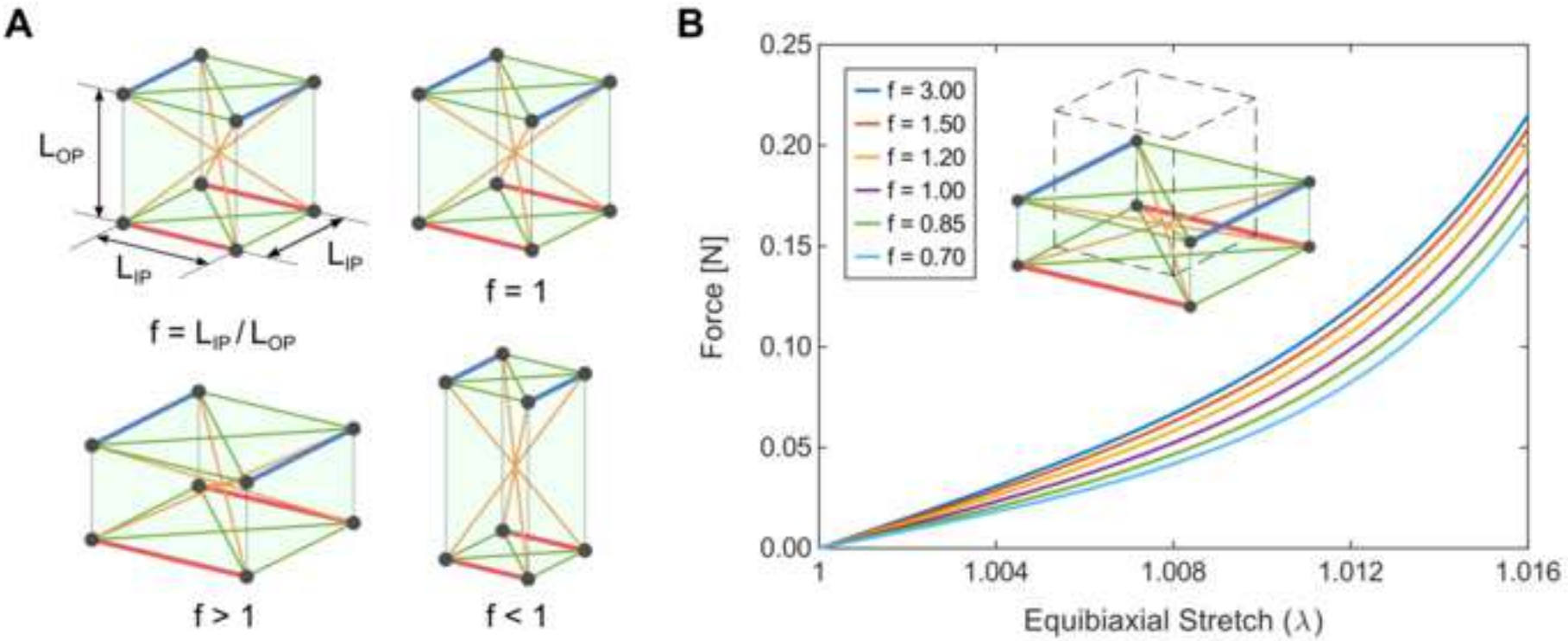

Figure 5

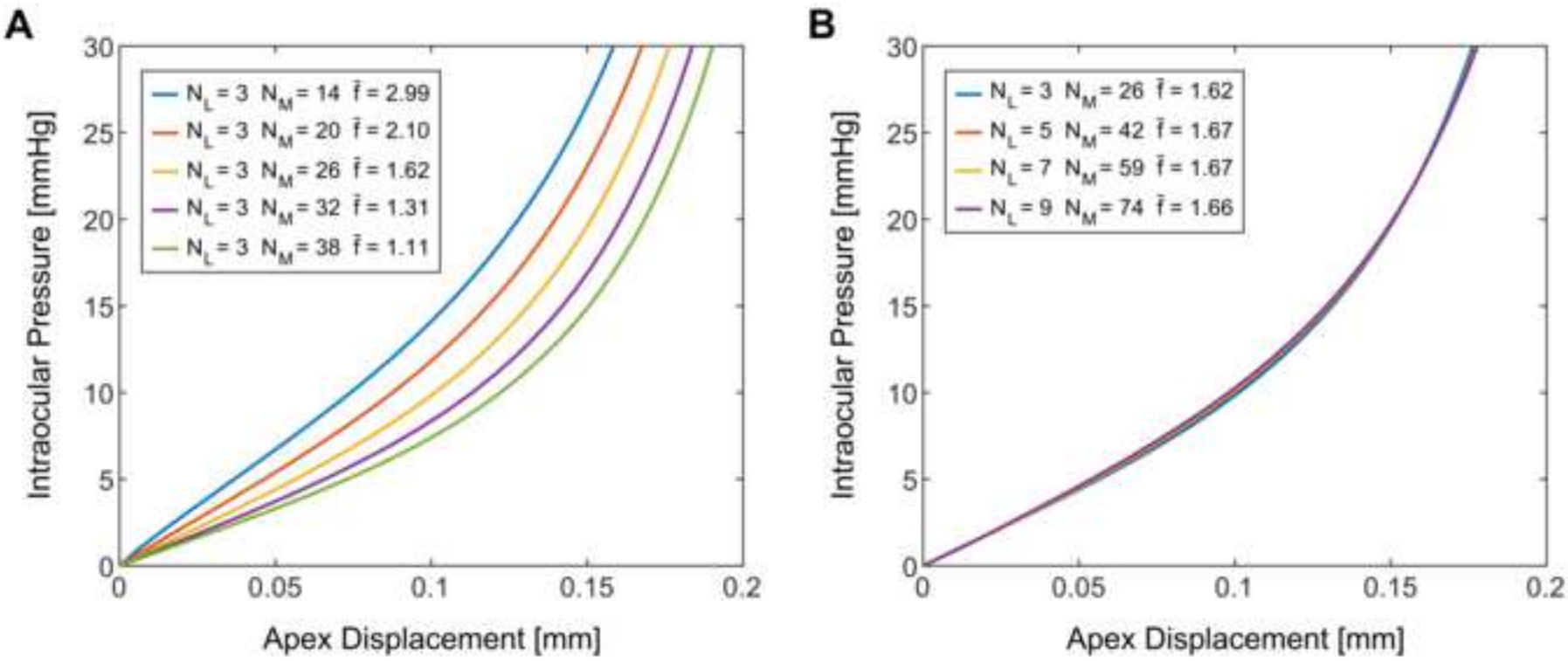

Figure 6

Click here to access/download;Figure;Figure6_w98_h73.png

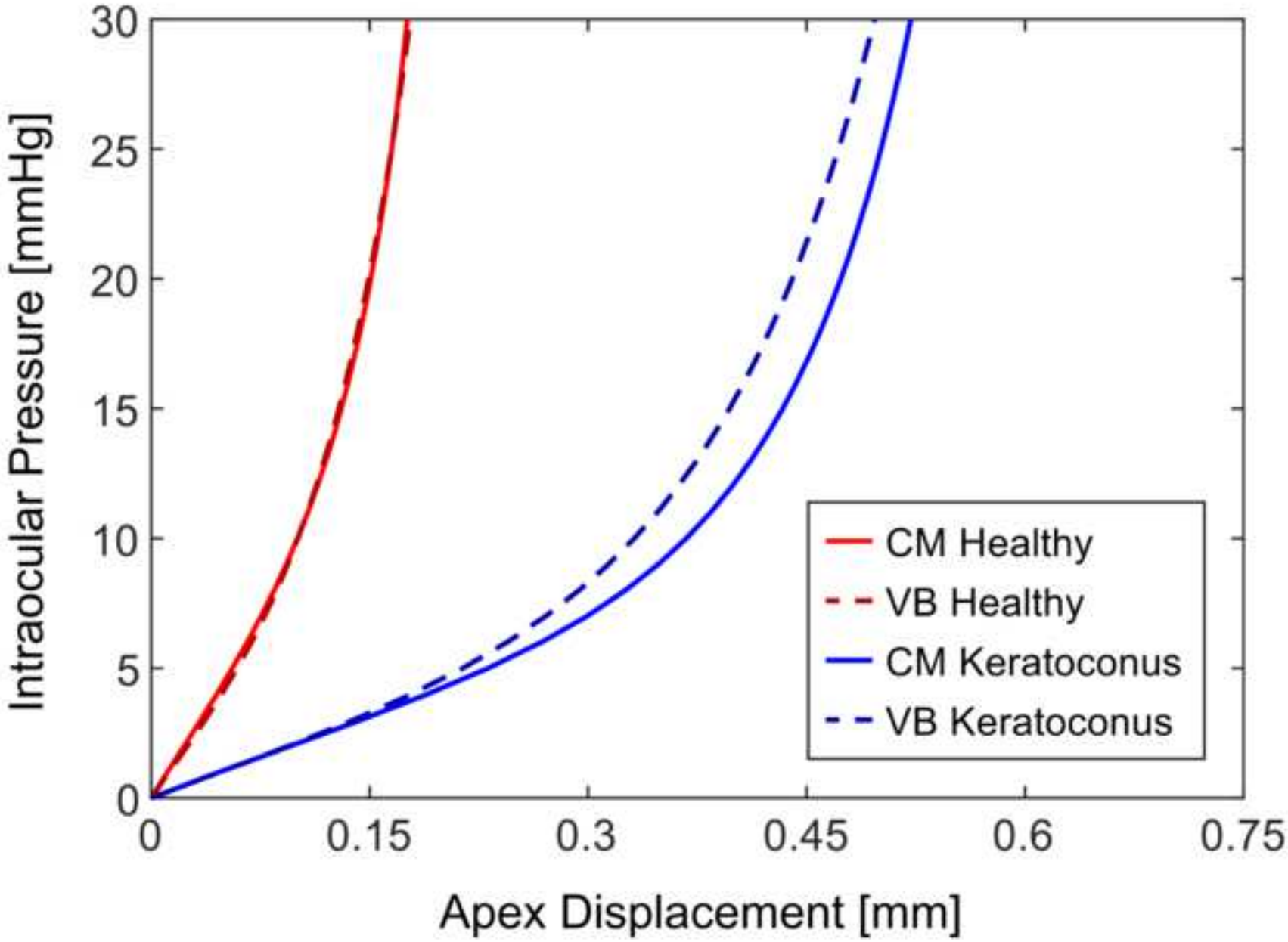

Figure 7

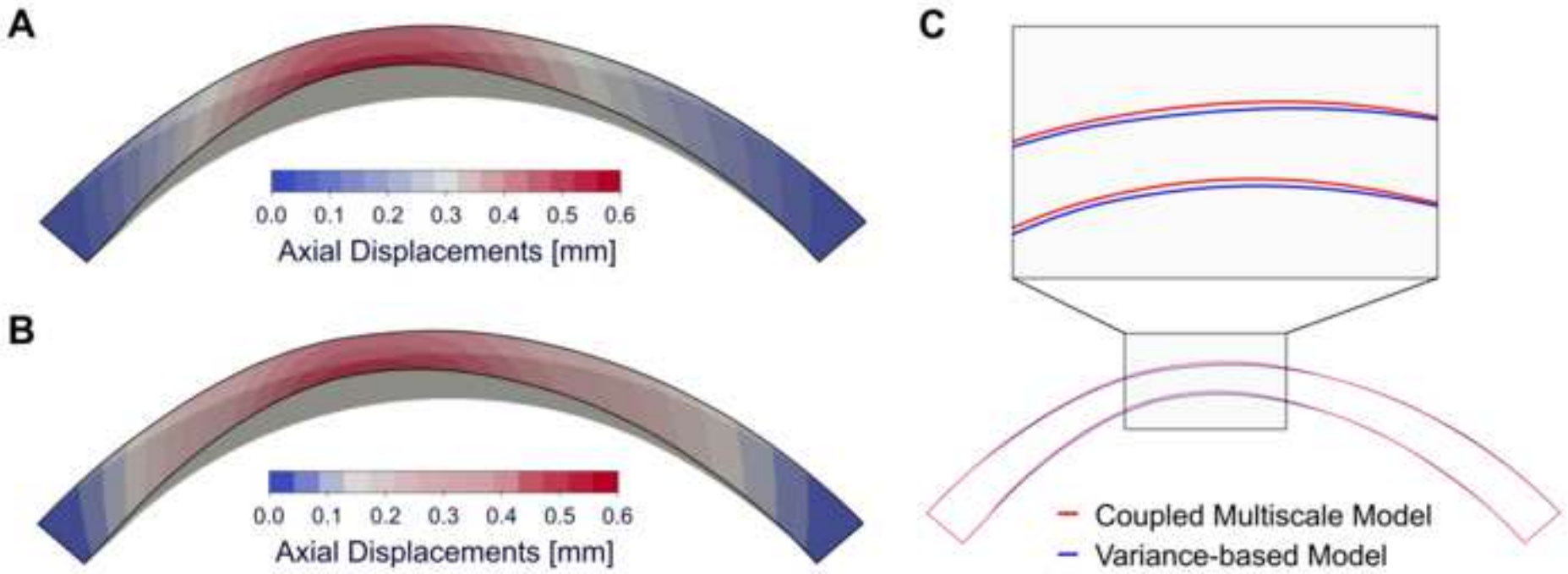

Declaration of interests

The authors declare that they have no known competing financial interests or personal relationships that could have appeared to influence the work reported in this paper.

Latex Source File

Click here to access/download

Latex Source File

sn-jnl.cls

Click here to access/download

Latex Source File

sn-chicago.bst

Click here to access/download

Latex Source File

sn-mathphys-num.bst

Click here to access/download

Latex Source File

sn-nature.bst

Click here to access/download

Latex Source File

sn-apacite.bst

Click here to access/download

Latex Source File

sn-aps.bst

A coupled multiscale model of the human cornea accounting for the collagenous microstructure and the extracellular matrix

Christopher Miller†, Maria Laura De Bellis[1]†, Anna Pandolfi[2*]†

[1]Department of Engineering and Geology, University of Chieti-Pescara, Viale Pindaro 42, Pescara, 10587, Italy.

[2*]Department of Civil and Environmental Engineering, Politecnico di Milano, Piazza Leonardo da Vinci 32, Milano, 20133, Italy.

*Corresponding author(s). E-mail(s): anna.pandolfi@polimi.it;

†These authors contributed equally to this work.

Abstract

The cornea is an ocular tissue that forms the clear outermost layer of the eye. Its highly specialized content and organization provide the cornea with mechanical properties that allow it to maintain its spherical shape under the action of intraocular pressure, a factor vital to its function within the eye's refractive system. We propose a coupled multiscale finite element model of the human cornea, where the tissue microstructure is upscaled in terms of a nonlinear trusswork of discrete structural elements, accounting for the stroma's distinctive collagen-crosslink lamellar architecture, and superpose it with continuum solid elements describing the non-collagenous extracellular matrix. As such, the cornea is regarded as a biological composite material with strongly nonlinear properties within a finite kinematics framework. The constitutive description is applied to a patient-specific geometry derived from corneal topography images, model parameters are calibrated to experimental pressure-inflation data, thus providing mechanical behavior representative of the healthy cornea, and the influence of the geometric discretization is also investigated. Most importantly, the presented framework is applied to the evolution of keratoconus, a pathology characterized by the localized protrusion and thinning of the cornea. We demonstrate that the outlined model, despite using relatively simplistic methods, albeit in a novel and innovative way, reproduces the formation of a conus to an extent more closely resembling clinical observations than previously reported approaches.

Keywords: Cornea, Biological composite, Continuum, Microstructural modeling, Collagen, Crosslinks

1 Introduction

The cornea is a quasi-spherical transparent shell occupying the outermost part of the eye, that covers the iris, pupil, and anterior chamber, see Fig. **??**A. Whilst it serves to protect the eye from infiltrates and ultraviolet radiation, the cornea's primary function is the refraction of light entering the eyeball. It is responsible for approximately two-thirds (43 diopters) of the eye's total optical power [**?**]. The cornea is made up of several distinct layers through its thickness, each fulfilling a specific role toward the overall functioning of the eye. However, it is the central stroma, making up 90% of the total volume, that dominates the biomechanical properties of the cornea. The stroma consists of a complex architecture of extracellular matrix (ECM) proteins whose specialized structure confers considerable tensile stiffness to the cornea. The tissue is hierarchically organized into numerous (≈300-500) lamellae running parallel to the corneal surface, each of which is composed of aligned bundles of collagen fibrils formed into ribbon-like sheets, with adjacent lamellae arranged at differing angles [**?**]. Throughout the collagenous microstructure, fibrils are interconnected by proteoglycan (PG) crosslinks which facilitate effective load-transfer and modulate fibril spacing through a careful balance of attractive-repulsive forces [**?**].

The analysis of the corneal microstructure via X-ray imaging has demonstrated that more than 60% of collagen fibrils have a randomly distributed orientation over the planes tangent to the mid-surface of the cornea, with the remaining 40% exhibiting a more characteristically orthogonal arrangement [**?**]. In the central cornea, collagen is clearly oriented in the nasal-temporal (NT) and superior-inferior (SI) directions, as a natural response to the activity of the eyelids and eye muscles [**?**]. Additionally, a prominent circumferential-radial alignment is seen at the periphery of the cornea where it connects with the sclera [**?**]. The local orthogonality of collagen fibrils is integral to the cornea's ability to sustain a mechanically-stable spherical shape under the action of an intraocular pressure of ≈ 16 mmHg and, critically, ensures the optimal deviation of the light rays onto the retina.

Clinical observations suggest that alterations to the cornea's collagenous architecture are linked to irreversible changes in its spherical geometry, disrupting the proper passage and refraction of light into the eye. A prominent example is keratoconus, a progressive non-inflammatory disorder where a loss in fibril organization leads to the cornea assuming a conical shape and thinning locally [**?**], see Fig. **??**B. This maladaptation can impair a patient's vision considerably, causing symptoms such as irregular astigmatism and high myopia. Additionally, abrupt changes in curvature may result in endothelial rupture, which can severely impact the regulation of the stroma's chemical composition. The etiology of keratoconus and the underlying processes driving its advancement are not fully understood, but its occurrence has been attributed to a range of biological, chemical, genetic, mechanical, and environmental factors [**?**].

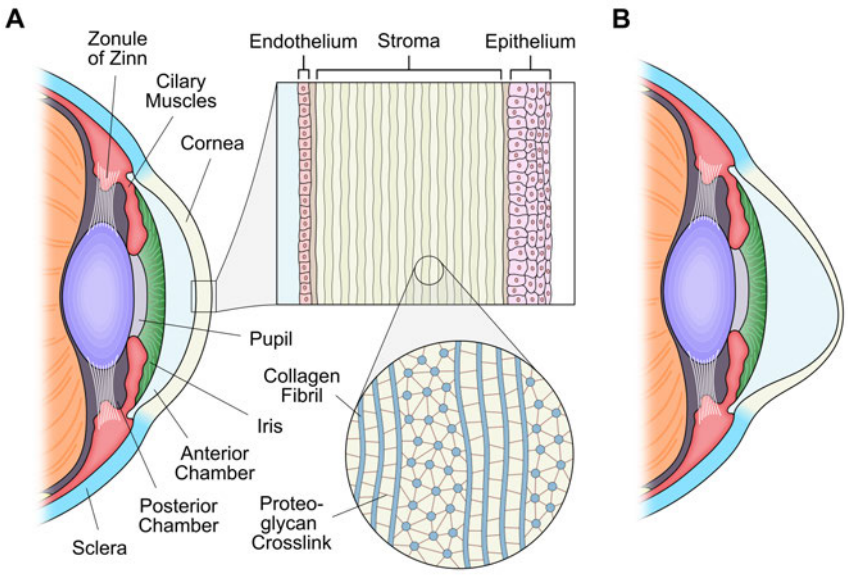

Figure 1 (A) A schematic diagram of the anterior segment of the eye, displaying the repeated structure of the cornea. A magnified view of the stroma demonstrates the organization of the collagenous microstructure into clearly defined lamellae consisting of differentially aligned collagen fibrils interconnected by proteoglycan crosslinks (not to scale). (B) An illustration of the keratoconic cornea, demonstrating the characteristic protrusion and thinning that are hallmark traits of the disease.

Given the many challenges that accompany the experimental assessment of the corneal microstructure, the identification of the deformation mechanisms underpinning healthy functionality and the changes corresponding to a diseased or damaged state are particularly troublesome [**?**]. Consequently, this has led to the pursuance of computational modeling methods aimed at reproducing the in vivo loading circumstances and replicating the mechanical behavior of the cornea. Beyond their use as a tool to bolster our comprehension of corneal mechanics, they hold great potential toward a host of clinical applications, either in the design and optimization of effective treatment strategies or through their direct introduction within the clinical workflow. Examples include the simulation of contact/contactless testing [**? ? ?**], the modeling of refractive surgeries (LASIK, SMILE, etc.) and surgical tools (Keratome, laser, etc.) [**? ? ?**], as well as predicting the progression of ectatic disorders such as keratoconus [**? ? ?**].

The majority of the numerical studies that have investigated the biomechanical response of the cornea have taken a continuum-based approach. Models of this kind have been employed extensively toward the modeling of numerous soft tissue types, as they can capture fundamental properties such as nonlinearity and anisotropy by accounting for tissue microstructure through a set of reinforcing fibers embedded within a continuum material, as well as other features such as fiber dispersion and spatially varying material stiffness [**? ? ? ? ? ?**]. Generally speaking, whilst it is clear

that continuum material descriptions of soft biological tissues can include the influence of mechanically significant proteins and deliver physiologically reasonable outcomes, they often fail to address how specific ECM components relate to each other on a structural basis. They provide a homogenized mechanical response and as such, do not readily integrate information concerning the positioning and combined organization of different constituents [**?**].

In the context of corneal modeling, continuum models are unable to suitably describe the complex interlinking of collagen fibrils via PG crosslinks, and how their functional interdependency gives rise to macroscopic tissue behavior. The characterization of collagen and crosslink mechanical properties is especially important in the case of models aimed at simulating the evolution of keratoconus, given the association of the pathology with degenerative changes to the collagenous microstructure. Continuum methodologies that have modeled conus formation through tissue weakening resulting from a region-specific temporal reduction of material stiffness have only been able to describe a moderate change in the cornea's spherical shape with limited localized thinning [**? ?**]. Models of this kind provide unsatisfactory results as they cannot adequately reflect the loss of structural integrity of the collagen skeleton.

These limitations have prompted the development of microstructurally-motivated discrete models in an effort to provide a more authentic portrayal of the cornea's architecture at sub-macro length scales, whereby the main structural components of the stroma, collagen and PG crosslinks, are explicitly incorporated within a three-dimensional network of structural trusses. The first deployment of this framework modeled all elements as linear elastic and, by simply manipulating the spatial allocation of the stiffness, produced realistic deformation profiles for the healthy and diseased cornea [**?**]. Subsequent versions examined more histologically appropriate constitutive relations, such as a more realistic pseudo-chemical Lennard-Jones potential to describe crosslink behaviour [**?**] and a collagen description encompassing the stochastic variation of the orientational dispersion of fibrils [**?**], with similarly successful outcomes. Other adaptations of the framework have introduced a damage-like scalar field whose evolution is governed by a reaction-diffusion equation [**?**]. This approach enables a spatial deterioration of element stiffness that can qualitatively predict conus formation.

The collective finding of the aforementioned studies has been the extent to which the weakening of chemical bonds between adjacent lamella heightens transversal shearing and compromises organ-level tissue stability, a feature consistent with experimental observations [**?**]. The increased deformability of the system leads to localized bulging, pronounced thinning and the reshaping of the cornea, providing a better geometric approximation of keratoconus compared to previous attempts. By directly incorporating key aspects of the microstructure and their impaired mechanical functionality, the various iterations of the outlined discrete modeling framework have demonstrated a substantial improvement in our ability to describe the development of keratoconus.

However, a notable shortcoming of this modeling strategy is that it only considers the reinforcing architecture of the cornea, i.e., it consists solely of struts representing fibrous collagen and associated crosslinks. Neglecting the ECM in which the collagenous microstructure is embedded renders this an incomplete and unrealistic

representation of corneal tissue. Going forward, if the true potential of this simple yet innovative approach is to be fully realized, the presence of the remaining non-collagenous isotropic ECM needs to be appropriately accounted for.

With this in mind, the present work proposes the superposition of the existing discrete microstructural framework with a continuous representation of the non-collagenous matrix, which is modeled as a classical hyperelastic Mooney-Rivlin material. Trusses representing generalized collagen fibrils and PG crosslinks are described by hyperelastic and Lennard-Jones models, respectively. This coupled multiscale modeling strategy, where the load-carrying function is provided by an autonomous structural network conforming to a filling continuum matrix, is an innovative approach, not just for the cornea, but for biomechanical applications in general.A modified finite element truss formulation is additionally presented, which correctly models the tissue microstructure by accounting for large deformation and material nonlinearity. The model is calibrated to provide mechanical behavior representative of the human cornea. The influence of the geometric discretization is investigated, and the ability of the model to characterize keratoconus is compared with previously reported computational models.

The organization of the manuscript is as follows. In Section (**??**), we introduce the geometry of the cornea, the constitutive models based on microstructural concepts, and the novel aspects of the finite element implementation. Numerical results are collected in Section (**??**), and a discussion of the proposed model, identifying its significance and potential applications, is reported in Section (**??**).

2 Materials and methods

2.1 Corneal geometry and microstructure

To arrive at clinically meaningful results, modern advanced computational models of the cornea are built directly from clinical data, whereby patient-specific geometries are constructed through the application of a sophisticated interpolation procedure to a cloud of surface points obtained from corneal topography images [**?**]. In general, coordinates are in reference to two axes that lie on the vertical plane orthogonal to the optic axis, x corresponding to the NT direction, and y corresponding to the SI direction, with the optic axis taken as the z axis. In the subsequent discussion, we refer to the NT-SI plane as the corneal plane. In this study, the chosen geometry is characterized by a set of shape-related parameters commonly referred to in a clinical setting, which are listed in Table **??**.

The geometry is discretized into hexahedral finite elements using an in-house developed 3D grid-generating software, where the discretization process is controlled by two parameters: the number of elements N_M along the principal meridian diameters (NT and SI), and the number of elements N_L across the thickness. An example of a generated mesh is provided in Fig. **??**A. The collagenous microstructure, assembled from a series of truss elements, is then superposed onto each solid element to form a unit cell, the configuration of which is detailed in Section (**??**).

The loading of the discretized geometry is provided by imposed tractions (Neumann boundary conditions) associated with the intraocular pressure at the posterior

Table 1 Geometric parameters relating to the anterior and posterior surfaces of the healthy cornea, described as two biconic surfaces. The reference plane contains the x (NT) and y (SI) axes of the model.

	Value	Unit
General		
Central thickness	0.57	mm
Apex elevation	2.48	mm
In-plane diameter	10.60	mm
In-plane orientation		
Steepest meridian NT	0	deg
Flattest meridian SI	90	deg
Anterior surface		
Steepest meridian radius	7.56	mm
Flattest meridian radius	7.41	mm
Asphericity coefficients	1.50	mm
Posterior surface		
Steepest meridian radius	6.47	mm
Flattest meridian radius	6.07	mm
Asphericity coefficients	1.00	mm

surface of the cornea. It is also necessary to impose the displacements (Dirichlet boundary conditions) at the external annulus of the geometry, i.e., the limbus, to properly account for the rotational freedom induced by the relative softness of the neighboring sclera and iris.

It should be noted that the measured geometry of the cornea relates to the tissue in its deformed state under the action of the intraocular pressure. As such, the entirely accurate modeling of the cornea using the finite element method necessitates the recovery of its unstressed configuration. Be that as it may, given the added complexity this would bring to the current study and the fact that our primary motivation is to demonstrate the efficacy and robustness of the presented coupled multiscale model, we simply treat the measured cornea as our referential geometry. This issue will, however, be addressed in future work through the integration of our previously developed inverse stress analysis scheme [**?**] within the modeling framework.

2.2 Unit cell definition

The microstructure of the cornea is characterized by the spatial repetition of a unit cell, where each unit cell consists of a solid 8-noded hexahedral finite element relating to the non-collagenous ECM material, and a series of truss elements interconnecting the various the nodes of the solid element, representing either a collagen fibril or a PG crosslink.

As illustrated in Fig. **??**B, we consider a unit cell to have two possible configurations, corresponding to whether it is located within an odd-numbered or an even-numbered layer, where a layer is defined as a group of unit cells existing at the

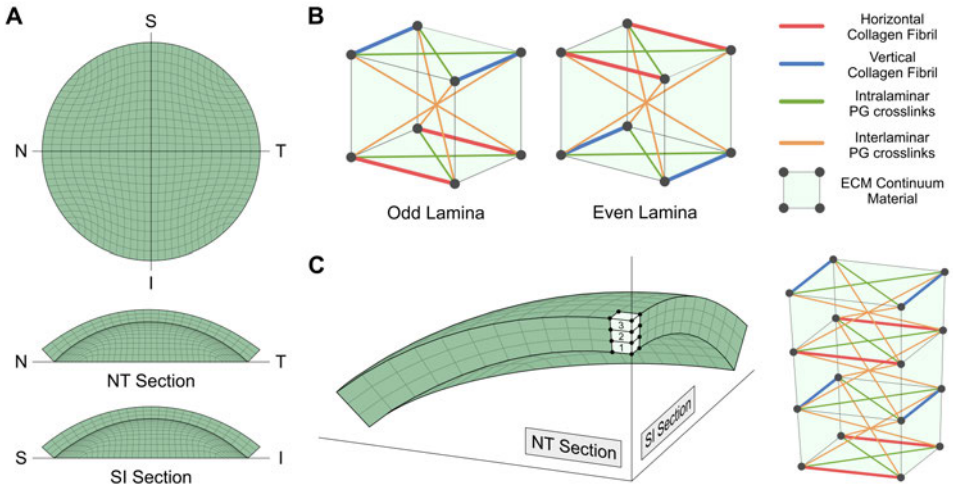

Figure 2 (A) An example of a finite element discretization of the human cornea, consisting of 2,500 nodes and 1,728 8-noded hexahedral elements. (B) The configuration of the unit cell characterizing the generalized microstructure of the cornea, with components describing collagen fibrils, PG crosslinks, and the remaining ECM. The multi-layer assembly of unit cells requires the distinction between those belonging to odd/even layers, so that the ideal organization of the stromal architecture is replicated. (C) An assembled mesh consisting of three unit cells across the thickness of the corneal geometry ($N_L = 3$), displaying the combined configuration of the three unit cells located at the apex, demonstrating how, over the entire geometry, this will lead to quasi-parallel surfaces of aligned collagen fibrils, (lamina), sequentially alternating in direction.

same depth through the thickness of the cornea. The first layer is on the posterior side of the cornea, whilst the number allocated to a layer increases successively in a posterior-to-anterior manner until the maximum is reached on the cornea's anterior side. An odd unit cell contains two vertical collagen trusses interspersed by two horizontal and two diagonal in-plane PG crosslinks located across its top surface, whereas the bottom surface contains two horizontal collagen trusses interspersed by two vertical and two diagonal in-plane PG crosslinks. Finally, four diagonal out-of-plane crosslinks link the nodes of the unit cells' top and bottom surfaces. An even unit cell is then simply the mirror of the odd unit cell in the z-axis. An example assemblage of several unit cells through the thickness of a three-layered discretized geometry is depicted in Fig. **??**C. It can be seen that in those instances where multiple adjacent unit cells contain entirely coincident trusses, we model only one truss element that belongs to all neighboring unit cells.

The configuration of unit cells in this way, when assembled to form the corneal geometry in its entirety, gives rise to quasi-parallel surfaces of aligned collagen fibril trusses separated equidistantly throughout the corneal thickness, which we will term laminae. The direction of alignment alternates sequentially in an approximately orthogonal fashion between the horizontal and vertical directions for each successive lamina. Therefore, in accordance with their hypothesized mechanical function, the

in-plane crosslinks act to distance the collagen fibrils within a lamina, whilst the out-of-plane crosslinks effectively separate neighboring laminae. From the arrangement of the PG crosslinks relative to the collagen fibrils, it is readily apparent that their presence will confer the generated trusswork with heightened structural stability compared to if they were absent.

In furtherance to the discussion of the geometric discretization procedure in the previous section, the mesh is generated in such a way that ensures the orientation of collagen truss elements properly reflects the spatial variation in collagen fibril direction (averaged across the thickness) as observed during the experimental imaging of the cornea [**?**]. Accordingly, the arrangement of the unit cells ensures that the main orientation of the fibrils gradually varies from an orthogonal arrangement at the center, which follows the NT and SI directions, to an orthogonal arrangement at the limbus, where fibrils run circumferentially and radially. Importantly, the regularity of the constructed mesh also ensures that this specific arrangement of the collagen and crosslink truss elements is maintained with increasing degrees of discretization along the principal meridian, N_M. Finally, to ensure an equal number of collagen fibril lamina aligned in the horizontal and vertical directions, the framework is restricted to the consideration of discretized geometries with an odd total number of layers, N_L.

All microstructural-based approaches require a set of assumptions to be made regarding the length-scales reflected in their mathematical framework, and the presented coupled multiscale model is no different. As the wholly realistic portrayal of the tissues' natural micro/nano-scales in a structural sense would require an inordinate number of elements, rendering any simulation far too computationally demanding, the approach taken is to instead assemble a network of trusses representing a more coarse *generalized* form of the collagenous architecture. The individual response of each truss element, in fact, corresponds to a collection of a given constituent. Modeling the hierarchical organization of collagen and PG crosslinks in this way, whilst a simplification compared to the ideal case, still retains our ability to investigate the structure-functional relationship of fibrillar collagen and PG crosslinks and how it imbues corneal tissue with its macroscopic mechanical stiffness and contributes to diseases such as keratoconus.

2.3 Constitutive descriptions

Here we detail the 1D constitutive descriptions of the generalized collagen fibrils and proteoglycan crosslinks, as well as the 3D continuum description accounting for the combined response of the remaining ECM constituents, which are not represented by the assembled trusswork.

2.3.1 Microstructural truss descriptions

The outlined descriptions consider each truss to be a hyperelastic body undergoing large deformations and, thus, employ finite kinematical theory. As such, the relative deformation measure used is the stretch λ, i.e., the deformed length l of the truss, divided by L, its undeformed referential length, where λ is considered to be uniform over the length of the truss. Furthermore, in keeping with experimental observations of

incompressibility concerning fibrous collagen and proteoglycans, we assume all trusses to conserve their volume when deformed.

Given that the traditional treatment of trusses is in a force versus displacement setting, by analogy and for convenience, the formulation is developed in the material reference frame, and therefore, the relations

$$P(\lambda) = \frac{\partial \psi}{\partial \lambda}\,, \quad \mathcal{A}(\lambda) = \frac{\partial P(\lambda)}{\partial \lambda} = \frac{\partial^2 \psi}{\partial \lambda^2}\,, \tag{1}$$

provide the scalar first Piola-Kirchhoff stress P, and the associated scalar stiffness $\mathcal{A}$, of a truss as a function of ψ, its potential energy. It is also worth noting that in the 1D case, P and λ represent an energetic conjugate pairing.

Collagen fibril

The material behavior of a truss representing a generalized collagen fibril is governed by a phenomenological constitutive description, well-established in the literature [**?**], which accounts for the nonlinear stiffening of soft tissues arising from the recruitment of undulated collagen fibrils. We begin by introducing a quadratic potential energy per unit volume acting along the length of the truss

$$\psi_{\text{coll}}(\lambda) = \frac{k_1}{2k_2}\left[\exp\left\{k_2\left(\lambda-1\right)^2\right\} - 1\right]\,, \tag{2}$$

where k_1 is the elastic stiffness of the fibril (with units of force per area) and k_2 is a dimensionless elastic rigidity parameter. The first Piola-Kirchhoff stress is then defined as

$$P_{\text{coll}}(\lambda) = \frac{\partial \psi_{\text{coll}}(\lambda)}{\partial \lambda} = k_1\left(\lambda-1\right)\exp\left\{k_2\left(\lambda-1\right)^2\right\}\,, \tag{3}$$

which in the absence of the exponential term would reduce to a standard neo-Hookean description. The stiffness is then found to be

$$\mathcal{A}_{\text{coll}}(\lambda) = \frac{\partial^2 \psi_{\text{coll}}(\lambda)}{\partial \lambda^2} = k_1\left[1 + 2k_2\left(\lambda-1\right)^2\right]\exp\left\{k_2\left(\lambda-1\right)^2\right\}\,. \tag{4}$$

which completes our 1D constitutive description for a generalized collagen fibril.

Proteoglycan crosslink

To characterize the mechanical response of the trusses representing the generalized PG crosslinks, we adopt a Lennard-Jones (LJ) potential. LJ models were initially conceived to describe the energy of two interacting objects as a function of the distance between them. They are able to capture the repulsive forces of particles (e.g., atoms, molecules) at close distances, the attractive forces at moderate distances, and the decay of interacting forces at infinite distances.

For this reason, they have also been used to represent the state of equilibrium existing in PG's and the role this plays in modulating the spacing of adjacent collagen

fibrils [**?**]. Specifically, PG's are prevented from assuming a fully extended conformation, which results in forces that tend to move fibrils closer together. However, PGs are hydrophilic, and the increased water volume leads to forces that push fibrils apart. A careful balance is reached, which in turn gives rise to specific interfibrillar distances.

To phenomenologically describe this behavior, we introduce a potential energy per unit volume of the form

$$\psi_{\text{pg}}(\lambda) = \varepsilon\lambda^{-a}\left(\lambda^{-a} - 2\right) , \tag{5}$$

where ε is the minimum potential energy per unit volume of the crosslink, i.e., the energy in the undeformed state, and a is a non-dimensional parameter. The first Piola-Kirchhoff stress is then denoted by

$$P_{\text{pg}}(\lambda) = \frac{\partial\psi_{\text{pg}}(\lambda)}{\partial\lambda} = 2a\varepsilon\lambda^{-(a+1)}\left(1 - \lambda^{-a}\right) , \tag{6}$$

where it is evident that the parameter, ε, dictates the peak stress of the crosslinks response, whilst a controls the change in stress with increasing axial deformation. The expression

$$\mathcal{A}_{\text{pg}}(\lambda) = \frac{\partial^2\psi_{\text{pg}}(\lambda)}{\partial\lambda^2} = 2\varepsilon a\lambda^{-2(a+1)}\left[2(a+1) - \lambda^a(2+a)\right] , \tag{7}$$

then details the corresponding stiffness and concludes the non-linear constitutive description for a generalized PG crosslink

2.3.2 Continuum extracellular matrix description

The continuum description of the isotropic ECM is determined according to the classical decoupled volumetric-deviatoric formulation of the strain energy density, thus ensuring that incompressibility, a focal feature of corneal tissue, is effectively enforced. The strain energy density is consequently given by

$$\Psi_{\text{ECM}} = \Psi_{\text{vol}}(J) + \Psi_{\text{iso}}(\bar{I}_1, \bar{I}_2) , \tag{8}$$

where Ψ_{vol} denotes a purely volumetric contribution that acts as a penalty term to impose the incompressibility constraint, and Ψ_{iso} is a purely isochoric contribution. The volumetric strain-energy takes the operative form

$$\Psi_{\text{vol}}(J) = \frac{K}{4}(J^2 - 1 - 2\log J) , \tag{9}$$

which depends on the Jacobian $J = \det\mathbf{F}$, where $\mathbf{F} = \partial\mathbf{x}/\partial\mathbf{X}$ is the deformation gradient. The coefficient K is related to the bulk modulus of the material, a suitably high value of which effectively preserves the volume at a Gauss-point [**?**].

An isotropic hyperelastic Mooney-Rivlin model [**?**] is assumed for the isochoric part of the deformation, based on its previous successful application to the cornea in

describing the ECM [**?**]. Accordingly, Ψ_{iso} is defined by the relation

$$\Psi_{\text{iso}}(\bar{I}_1, \bar{I}_2) = \frac{\mu_1}{2}(\bar{I}_1 - 3) + \frac{\mu_2}{2}(\bar{I}_2 - 3)\,, \tag{10}$$

with $\mu = \mu_1 + \mu_2$ denoting the shear modulus of the material, $\bar{I}_1 = \text{tr}(\overline{\mathbf{C}})$ and $\bar{I}_2 = [(\text{tr}(\overline{\mathbf{C}}))^2 - \text{tr}(\overline{\mathbf{C}}^2)]/2$, corresponding to the first and second invariants of the modified right Cauchy-Green deformation tensor, itself described by, $\overline{\mathbf{C}} = \overline{\mathbf{F}}^{\text{T}}\overline{\mathbf{F}}$, where $\overline{\mathbf{F}} = J^{-1/3}\mathbf{F}$ is the modified deformation gradient.

2.4 Finite element formulation

The aspects of the finite element formulation relevant to the present multiscale model of the cornea are briefly recalled. All simulations are carried out using a specifically designed in-house software coded in the programming language C.

2.4.1 Truss elements

We begin by considering a truss element consisting of two nodes $\{\text{a}, \text{b}\}$ whose referential and deformed coordinates are given by the two sets of vectors $\{\mathbf{X}_\text{a}, \mathbf{X}_\text{b}\}$ and $\{\mathbf{x}_\text{a}, \mathbf{x}_\text{b}\}$, respectively. Consequently, the relation $\mathbf{u}_{(\bullet)} = \mathbf{x}_{(\bullet)} - \mathbf{X}_{(\bullet)}$ provides the displacement vector for a given node.

Following on from the constitutive descriptions outlined in Section (**??**), the internal forces acting at each node of the truss are denoted by

$$\mathbf{T}_\text{a} = -P(\lambda)A\ \mathbf{n}\,, \quad \mathbf{T}_\text{b} = P(\lambda)A\ \mathbf{n}\,, \tag{11}$$

where A is the referential cross-sectional area, $\mathbf{n} = (\mathbf{x}_\text{b} - \mathbf{x}_\text{a})\,/l$ is a unit vector defining the deformed truss's three-dimensional direction in space, and $P(\lambda)$ is the first Piola-Kirchhoff stress of the truss.

The linearization of the equilibrium equations for each node with respect to the two displacement vectors ultimately yields a set of linear equations for an element, which in matrix representation reads

$$\begin{bmatrix} \mathbf{T}_\text{a} \\ \mathbf{T}_\text{b} \end{bmatrix} = \begin{bmatrix} \mathbf{K}_\text{aa} & \mathbf{K}_\text{ab} \\ \mathbf{K}_\text{ba} & \mathbf{K}_\text{bb} \end{bmatrix} \begin{bmatrix} \mathbf{u}_\text{a} \\ \mathbf{u}_\text{b} \end{bmatrix}. \tag{12}$$

The individual contributions to the element tangent stiffness matrix relate the change in the forces at a node to the change in the current position of a particular node. Each contribution is defined according to the relations

$$\mathbf{K}_\text{aa} = \mathbf{K}_\text{bb} = [\alpha(\lambda) - \beta(\lambda)]\,(\mathbf{n} \otimes \mathbf{n}) + \beta(\lambda)\mathbf{I}\,, \quad \mathbf{K}_\text{ab} = \mathbf{K}_\text{ba} = -\mathbf{K}_\text{aa}\,, \tag{13}$$

where $(\mathbf{n} \otimes \mathbf{n})$ is a second-order unit structural tensor containing the trusses' directional information, and $\mathbf{I}$ denotes the identity tensor. The two terms in Eq. (**??**a) are analogous to the constitutive and geometric quantities arrived at when deriving the

tangent stiffness matrix for a solid finite element. The deformation-dependent scalars, $\alpha(\lambda)$ and $\beta(\lambda)$, have the units, force per unit length, and are defined by the expressions

$$\alpha(\lambda) = \frac{\mathcal{A}(\lambda)A}{L}\,, \quad \beta(\lambda) = \frac{P(\lambda)A}{l}\,. \tag{14}$$

Their derivation, arising from the directional derivative of the internal truss forces in the material frame, is provided in Appendix **??**. The formulation differs from the classical non-linear truss formulation [**?**] in that, in addition to being alternatively derived in the material frame, the strain measure employed is the axial stretch of the structural element, ensuring that it is better suited towards characterizing the large deformation of the reinforcing collagenous trusswork.

As was detailed in Sec. **??**, all trusses are generalized and thus characterize a collection of a given structural protein. Specifically, the unit cell, the fundamental building block of the corneal model, represents the up-scaling of low-scale microscopic components to the macroscale [**?**]. Thus, each truss element must account for a certain quantity of the tissue material, which reduces proportionally with the size of the discretization. This can be facilitated in a straightforward way by modifying the referential cross-sectional area A allocated to each element. The internal forces and the tangent stiffness matrix contribution of each truss element are assumed to be a function of both N_M, the number of unit cells along the principal meridian, and N_L, the number of unit cells across the thickness. Thus, the area of all trusses in the assembled meshwork is defined as

$$A = w_M w_L \overline{A} \tag{15}$$

where $w_M = 1/N_M$ and w_L are scalar weighting factors referring to the meridian and thickness discretization, respectively. Note that the collagen and crosslink trusses located entirely (both nodes) on the anterior or posterior surfaces are allocated a weighting of $w_L = 1/2N_L$, whilst the remaining majority of the trusses are allocated a weighting of $w_L = 1/N_L$. As the cross-sectional area carries no explicit physiological meaning, we set the input parameter $\overline{A} = 1$ for all trusses such that the mechanical properties of each truss are then fully encapsulated by their respective constitutive parameters.

2.4.2 Solid elements and boundary conditions

To model the ECM continuum material, we used standard linear 8-noded hexahedral isoparametric elements, whose formulation is well-established in the literature and can be found in standard textbooks, e. g., [**?**].

The intraocular pressure exerted by the aqueous humor is assumed to act uniformly over the posterior surface of the cornea and to act exclusively on the posterior facets of the solid elements, since the collagen/crosslinks trusses cannot be loaded transversally. The pressure is translated into equivalent nodal forces by using the energetic equivalence that arises from the weak form of the linear momentum balance used in the Galerkin approach. The intraocular pressure acts in the direction normal to the

posterior surface, and as such, the external loading of the system is a function of the cornea's current deformation state and must be recomputed at every time step.

Concerning the displacement boundary conditions at the limbus, previous numerical studies have demonstrated that the dominant mechanical effect of surrounding tissues upon the cornea is that they limit the occurrence of bending moments. We therefore enforce that the cross-section of the cornea at the limbus preserves orthogonality conditions with respect to the deformed mid-section of the shell, reducing the engagement of the tissue in terms of stored energy, an aspect that complies with the concept of energy minimization governing the behavior of biological homeostasis.

2.4.3 Solution methodology

The solution of the quasi-static non-linear problem of the pressurized cornea requires the introduction of a simulation time-frame, $t_n = t_{n-1} + \Delta t$, where Δt is the incremental time step. The finite element spatial discretization of the linear momentum equation leads, following assembly, to a non-linear algebraic system of equations that, at the time t_n, can be written in the form

$$\mathbf{R}_n(\mathbf{u}_n) = \mathbf{T}_n(\mathbf{u}_n) - \mathbf{F}_n \to \mathbf{0}\,, \tag{16}$$

where $\mathbf{T}_n(\mathbf{u}_n)$ is the global internal forces array, $\mathbf{u}_n$ is the global displacement array, and $\mathbf{F}_n = \mathbf{F}_{n-1} + \Delta\mathbf{F}$ is the global external forces array, with the residual array $\mathbf{R}_n(\mathbf{u}_n)$ becoming $\mathbf{0}$ only when equilibrium is satisfied.

In this modeling framework, two solution strategies are implemented, the first of which is the traditional Newton-Raphson method. Linearization of the residual array introduces the tangent stiffness matrix and accompanying set of equations, which read

$$\mathbf{K}_n^k = \frac{\partial \mathbf{R}_n^k}{\partial \mathbf{u}}\,, \quad \mathbf{u}_n^{k+1} = \mathbf{u}_n^k - \left[\mathbf{K}_n^k\right]^{-1} \mathbf{R}_n^k\,,$$

and are solved iteratively at each time point t_n, until global equilibrium, i.e., Eq. (**??**), is satisfied to a predefined tolerance.

However, given the definition of a unit cell, the proposed multiscale model requires a significant number of elements for even moderately discretized corneal geometries, and the resulting size of the global tangent stiffness matrix can become very large, rendering the simulation cumbersome and computationally expensive. Furthermore, this model was conceived with its application towards the simulation of corneal degeneration in mind. For such problems, progressive tissue softening can potentially lead to accompanying, often severe, numerical issues when using the Newton-Raphson scheme. A more convenient approach is therefore to utilize the dynamic relaxation method [**?**], where we instead construct a critically damped pseudo-dynamic problem described with a fictitious time $\tilde{t}$ (independent of the timescale of the simulation), defined by the expression

$$\mathbf{R}_n(\mathbf{u}_n) = \mathbf{M}_{\text{fict}}\ddot{\mathbf{u}}_n(\tilde{t}) + \mathbf{D}_{\text{fict}}\dot{\mathbf{u}}_n(\tilde{t}) + \mathbf{T}_n(\mathbf{u}_n, \tilde{t}) - \mathbf{F}_n \to \mathbf{0}\,, \tag{17}$$

and designed for the fastest possible convergence toward the steady-state solution. The internal variables, $\dot{\mathbf{u}}$ and $\ddot{\mathbf{u}}$ are the nodal velocity and acceleration arrays, and $\mathbf{M}_{\text{fict}}$ and $\mathbf{D}_{\text{fict}}$ are the fictitious diagonal mass and damping arrays. The pseudo-dynamic problem in Eq. (**??**) is numerically integrated with respect to $\tilde{t}$ until the steady-state solution is reached ($\ddot{\mathbf{u}} = \dot{\mathbf{u}} = \mathbf{0}$) and global equilibrium is satisfied to a predefined tolerance.

The pseudo-time $\tilde{t}_k = \tilde{t}_{k-1} + \Delta\tilde{t}$ at each iteration of the dynamic relaxation method is defined by $\Delta\tilde{t}$, an arbitrary chosen pseudo-time step. Since the actual density of the material is not relevant in the static problem, for each solid element the pseudo-time step is used to define an ideal density ρ_e such that the critically stable time step Δt_e, defined by the Courant–Friedrichs–Lewy dynamic stability condition, coincides with the chosen $\Delta\tilde{t}$. For a given element size h_e, the critical Δt_e is defined as

$$\Delta t_e = \frac{h_e}{c_e} \approx h_e \sqrt{\frac{\rho_e}{E_e}} = \Delta\tilde{t} \quad \rightarrow \quad \rho_e = E_e \frac{\Delta\tilde{t}^2}{h_e^2}\,, \tag{18}$$

where c_e is the longitudinal wave speed of the material and E_e is the *average* elastic modulus of the element. The element mass matrix is then obtained via the Galerkin approximation by using the element interpolation functions, row lumped to facilitate the numerical solution.

The damping matrix $\mathbf{D}_{\text{fict}}$ is assumed to scale linearly with $\mathbf{M}_{\text{fict}}$ by a weighting factor $\alpha \approx 2\omega_0$, where ω_0 is the first eigen-frequency of the discretized system, approximated by the stiffness-mass Rayleigh ratio

$$\omega_0{}^2 = \max\left(\frac{\mathbf{du}^{\mathrm{T}}\left[\mathbf{T}_{\mathrm{k}} - \mathbf{T}_{\mathrm{k-1}}\right]}{\mathbf{du}^{\mathrm{T}}\mathbf{M}_{\text{fict}}\mathbf{du}}, 0\right), \tag{19}$$

which has been modified specifically for the dynamic relaxation method [**?**].

It is worth commenting briefly on the choice of the solver. The dynamic relaxation method has been proven to be numerically advantageous in conditions of material softening, as well as in managing contact and self-contact. In such instances, it is superior to other Newton-Raphson based algorithms for two main reasons: (i) it deals easily with strong nonlinearities, since it naturally discriminates between multiple solutions to obtain the stable one, and (ii) and it can be optimally implemented in concurrent computers, as the pseudo-dynamic system of equations reduces to a set of independent equations. Whilst Newton-Raphson requires a small number of expensive iterations (on the order of 10), dynamic relaxation requires many inexpensive iterations (on the order of 1000). Moreover, in terms of scalability regarding the mesh size, for a discretized system with N degrees-of-freedom, standard Newton-Raphson algorithms scale as $O(N^{1.5}) - O(N^2)$, whereas dynamic relaxation algorithms scale as $O(N)$, thus demonstrating a clear computational advantage when it comes to larger meshes.

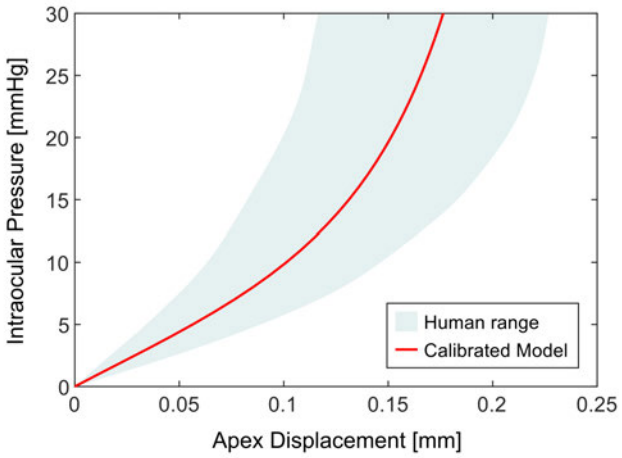

Figure 3 Calibrated mechanical response of the presented multiscale model for the cornea under the action of the intraocular pressure. The model was fitted to the mean mechanical response of the ex vivo pressure inflation experimental data reported in [**?**], for which the range of biological variability is also shown.

3 Results

3.1 Constitutive parameter calibration

When computationally modeling soft biological tissues, patient-specific geometries can only confer physiologically predictive results by also establishing the corresponding patient-specific material parameters. Unfortunately, in the context of the human cornea, the lack of suitable in vivo mechanical tests that can differentiate the response of the cornea from that of the overall system (eyeball) renders the determination of the tissue's exact constitutive properties a challenging feat. However, to arrive at reasonable numerical results that are realistic to the human cornea, we start by calibrating the proposed multiscale model to experimental data concerning the ex vivo pressure inflation testing of the isolated cornea [**?**]. The testing protocol implies the complete blockage of the sclera adjacent to the limbus and the progressive increase of the applied intraocular pressure from 0 to 30 mmHg. A corneal geometry with discretization parameters $N_L = 3$ and $N_M = 26$ was used for the fitting. The identified set of constitutive parameters is reported in Table **??**, and the mechanical response reached is shown in Fig. **??**, demonstrating that the model successfully captures the mean mechanical behavior over the experimental range of variability. The calibrated parameters have been used in the numerical calculations described later.

We note that the second stiffness coefficient of the Mooney-Rivlin model, used to describe the extracellular matrix, is negative. In general, this choice must be carefully verified, since it can lead to the global instability of the strain energy. However, since our early work concerning the human cornea, we have made this choice for the characterization of the extracellular matrix, in order to capture the low stiffness of the

structure observed at low values of the intraocular pressure [**?**]. The particular loading conditions (pressurization) and the presence of reinforcing fibers help in avoiding stability issues, and no anomalous behavior has been observed in all our numerical tests.

Table 2 Parameters obtained following the calibration of the model to human cornea pressure inflation testing data [**?**], where discretization parameters of $N_L = 3$ and $N_M = 26$ were used. The table also includes the calibrated parameters for the variance-based model used for comparative analysis [**?**].

		Value	**Unit**
Coupled multiscale model			
Truss elements			
Referential cross-sectional area	$\overline{A}$	1.00	mm^2
Collagen fibril			
Elastic Stiffness	k_1	1.8	MPa
Rigidity Parameter	k_2	4000	
Proteoglycan crosslink			
Minimum Potential energy	ε	0.01	MPa
Exponent	a	6	
Solid elements			
ECM continuum material			
Shear modulus 1	μ_1	0.0015	MPa
Shear modulus 2	μ_2	-0.0014	MPa
Bulk modulus	K	5	MPa
Variance-based model (two fibril families)			
Solid elements			
Anisotropic collagen-related contribution			
Fibril stiffness parameter (both families)	k_1	0.2	MPa
Fibril rigidity (both families)	k_2	510	
Dispersion coefficient (both families)	κ	location dependent	
Isotropic contribution			
Shear modulus 1	μ_1	0.0015	MPa
Shear modulus 2	μ_2	-0.0014	MPa
Bulk modulus	K	5	MPa

3.2 Influence of the geometric discretization

As the proposed model incorporates a combination of both truss and solid finite elements to upscale the microstructural features of corneal soft tissue to the macroscale, it is necessary to investigate how the geometric discretization impacts the obtained numerical results.

As depicted in Fig. **??**A, a unit cell has three dimensions, an out-of-plane height L_{OP}, and two in-plane dimensions. The method of discretization for the corneal geometry ensures that for all the generated unit cells, the two in-plane dimensions are

always approximately equal, and so we use the average in-plane dimension L_{IP} to represent both. A shape factor $f = L_{IP}/L_{OP}$ can then be defined, which provides pertinent information relating to the relative dimensions of a given unit cell, cf. [**?**]. For instance, a value of $f = 1$ refers to a referential cubic unit cell, whilst values of $f < 1$ and $f > 1$ refer to referential dimensions that are elongated in the out-of-plane and in-plane directions, respectively.

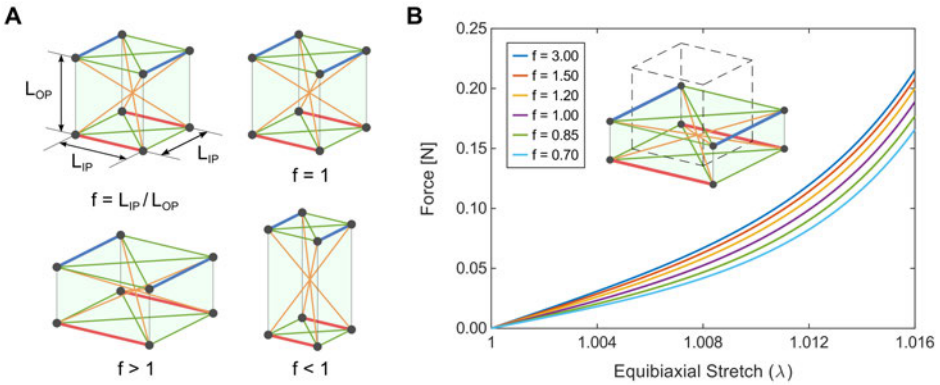

Figure 4 (A) Diagram illustrating the definition of the shape factor f, as well as representative examples of the referential state for the cases of $f = 1$, $f > 1$, and $f < 1$. (B) The mechanical response of a single unit cell exposed to planar equibiaxial tension, for varying values of f, including a diagram showcasing the referential and deformed states for the case of $f = 1$.

The influence of the shape factor f upon the behavior of a single unit cell exposed to planar equibiaxial tension, a loading circumstance closely resembling that of the unit cell in the full organ-level problem, can then be examined. The referential cross-sectional area of the facets over which the force is applied is kept the same for each test to ensure that the continuum ECM force contribution remains the same. From Fig. **??**B, it can be seen that for decreasing values of f, the response softens, which is a consequence of the diagonal trusses within the unit cell representing the PG crosslinks. For different values of f, these trusses experience a different axial elongation for the same biaxial deformation of the unit cell, and as such, provide a different contribution to the overall force.

Next, we focus our attention on the effect of the discretization parameters, N_L and N_M, on the mechanical behavior of the pressurized cornea, as the choice of said parameters will obviously dictate the shape of the unit cells that make up the corneal geometry as a whole. This impact is measured through the average value of the shape factor $\bar{f}$ across all resident unit-cells, allowing for an effective comparison of the different degrees of discretization. From Fig. **??**A, it can be seen that the influence of the relative dimensions observed for a single unit cell also manifests at the whole organ-level. The number of layers is held constant at $N_L = 3$, whilst the value of N_M is altered. For more elements across the meridian diameter, the magnitude of $\bar{f}$

decreases, and there is a corresponding reduction in the cornea's macroscopic stiffness. From Fig. **??**B it is evident that if N_L and N_M are chosen to provide values of $\bar{f}$ that are approximately equal in magnitude, the mechanical behavior of the cornea is relatively consistent, with the minor discrepancies also likely attributable to standard mesh convergence phenomena.

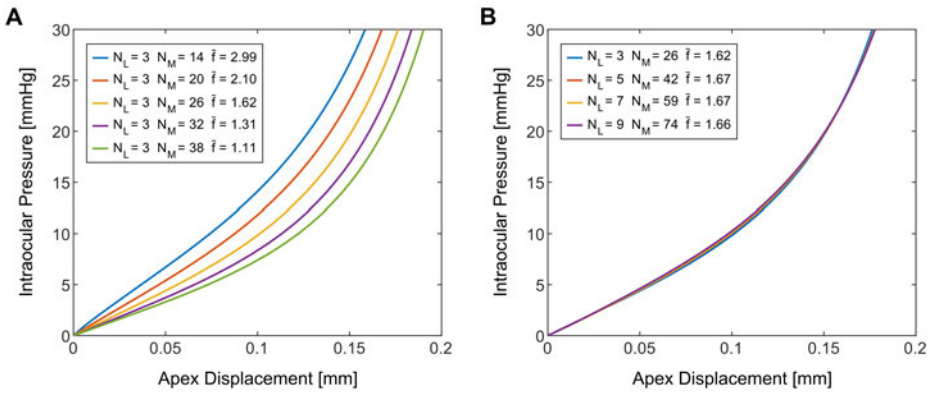

Figure 5 (A) Simulations for differing values of the discretization parameters N_L and N_M that give varying magnitudes of $\bar{f}$ and therefore alternate mechanical behaviors. (B) Simulations for differing values of N_L and N_M that are specifically chosen to give approximately equal magnitudes of $\bar{f}$ and therefore correspondingly equivalent mechanical behavior.

3.3 Application of the model to Keratoconus

The proposed coupled multiscale model has the potential to describe the mechanical outcome of pathologies such as keratoconus, which are characterized by a reduction in material stiffness within a localized area of the cornea, leading to the development of a distinct conical shape. To assess the model's ability to simulate keratoconus, we compare its prediction with that of a phenomenological variance-based continuum model of the corneal stroma, previously applied to the simulation of mechanical tests and refractive surgery procedures [**?**]. It accounts for the reinforcement of the collagenous matrix via two families of dispersed collagen fibrils, obeying a von Mises orientation distribution governed by a scalar parameter $b(\mathbf{x})$, itself a function of the spatial location within the cornea. The model employs the average and variance of the fourth pseudo-invariant $\overline{I}_4^*$, coupling the orientation of a single fibril to the deformation gradient. As with the coupled multiscale model, we calibrate its material parameters to experimental pressure inflation data (Table **??**), such that the mechanical response of both models are approximately equivalent for the healthy eye. Note that both models use the Mooney-Rivlin strain energy function to describe the isotropic ECM material. A brief overview of the variance-based model is provided in Appendix **??**.

To model the degeneration of the corneal stroma, the various stiffness parameters of both models are reduced according to a scalar damage field $d \in \{0, 1\}$. Clearly, the reduction is not applied to the bulk modulus K, which acts as a penalty coefficient to enforce incompressibility. The spatial distribution of d is assumed to be quadratic and to cover a circular area of radius R = 4 mm, with maximum tissue degeneration ($d = 1$) at the center and no degeneration ($d = 0$) at the boundary of the damaged zone, cf. [**?**]. The center of the allocated damage field is situated 1 mm towards the inferior side of the cornea, along the SI meridian, in agreement with clinical evidence indicating that keratoconus tends to localize in the lower portion of the corneal surface [**?**].

The global mechanical response under the action of the intraocular pressure, for the proposed coupled multiscale model and the variance-based model, applied to the healthy and keratoconus cases, is shown in Fig. **??**. Whilst the two models predict the same behavior under healthy conditions, they differ for the keratoconus case, with the coupled multiscale model exhibiting greater compliance.

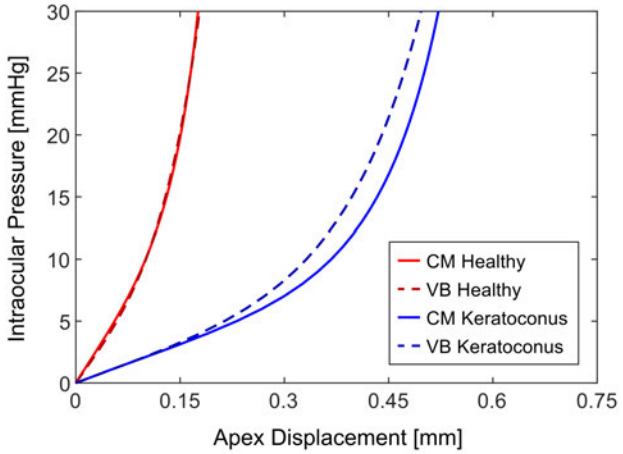

Figure 6 The mechanical response of the presented Coupled multiscale (CM) model and the Variance-based (VB) Model for both the healthy (calibrated to experimental data [**?**]) and keratoconus case.

SI meridian sections of the cornea are displayed in Fig. **??**, demonstrating that both models are able to capture the key features of the pathological configuration. Specifically, Fig. **??**A compares the profiles of the healthy and keratoconus corneas obtained with the coupled multiscale model, whilst Fig. **??**B compares the same profiles obtained with the variance-based model.

A direct comparison between the keratoconus profiles predicted by the two models is provided in Fig. **??**C. The conical protrusion appears slightly more pronounced in the coupled multiscale model, which reveals $\approx 7\%$ higher displacements at the corneal apex. Moreover, a more pronounced thinning is observed in the region of the conus apex, suggesting a more marked stiffness reduction.

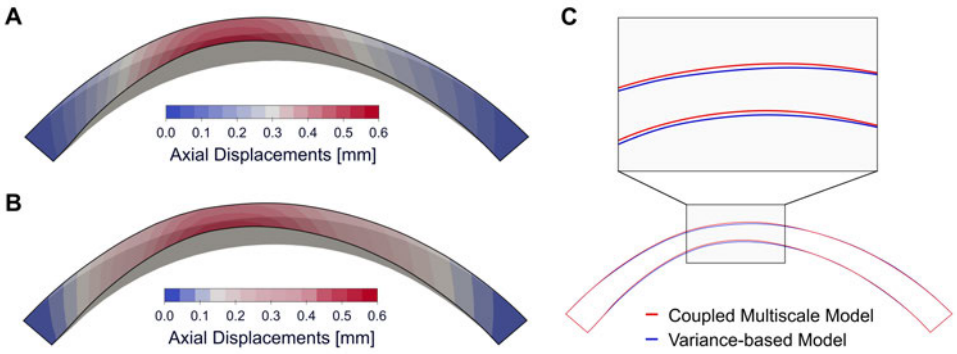

Figure 7 (A) SI meridional profile of the cornea under healthy and keratoconus conditions obtained with the coupled multiscale model. The keratoconus configuration is highlighted with a colour map visualizing the displacements along the optic axis. A conical protrusion has formed, characteristic of keratoconus, with a localized narrowing at the location of maximum damage. (B) SI meridional profile of the cornea under healthy and keratoconus conditions obtained with the variance-based continuum model. Whilst a localized bulging occurs, the deformation is less pronounced than that obtained with the coupled multiscale model. (C) Direct comparison of the SI profile of the keratoconus corneas at physiological intraocular pressure (15 mmHg), obtained with the coupled multiscale and the variance-based models.

4 Discussion and conclusions

In recent times, the computational modeling of biological systems has become a vital tool in supporting the design of surgical and pharmacological treatments. Despite the difficulties associated with the selection of in vivo physical properties, numerical models can, for instance, be used to simulate surgical procedures and augment clinical awareness regarding optimal outcomes, especially when the surgery is risky. They are also becoming increasingly relevant in the study of disease, elucidating the myriad factors linked to the incidence and progression of corneal pathologies. In silico modeling could therefore be the key to solving, or at least partially alleviating, the various mysteries of corneal biomechanics.

Advanced continuum-based numerical models of the human cornea have been successfully deployed in the simulation of healthy physiological states [**?**], in vivo mechanical tests [**? ? ?**], and surgical procedures [**? ? ?**]. Nevertheless, such approaches, which often disregard the underlying microstructure, have proven to be insufficient in the modeling of tissue degeneration [**? ?**]. Recently, a micromechanical approach upscaled to the organ level has been successfully applied to model the evolution of keratoconus [**? ?**]. The approach explicitly accounts for the mechanical interaction of salient features such as fibrous collagen and associated crosslinks by characterizing them as structural truss elements within a spatially repeating unit-cell, which defines the load-carrying lamellar structure of the stroma, thus providing a more physical interpretation of the microstructure compared to entirely phenomenological continuum models.

This study has been devoted to the extension of this existing discrete framework to further include a continuum representation of the non-collagenous ECM in which the mechanically significant constituents are embedded. With the framework now amended to treat the cornea as a solid entity, this multiscale approach now correctly enforces material incompressibility, a hallmark feature of soft biological tissues. It is also well-placed for the possible integration of mathematical descriptions accounting for coupled phenomena such as heat conduction during surgical treatments and fluid/ion fluxes occurring at the posterior surface to preserve corneal transparency. Importantly, the superposition of the collagen trusswork and the ECM continuum within a finite element discretization is computationally straightforward, and the amalgamation of the two approaches has the potential to overcome the fundamental failings of either alone.

The coupled multiscale model presented in this study is an innovative and versatile framework that explicitly models collagen and crosslink components as distinct structural elements, accounting for the organization of fibrous collagen into a lamellar structure, as well as the spatial arrangement and orientation of fibrils throughout the cornea. To the best of our knowledge, no approach has been applied previously that has upscaled the microstructure in terms of a nonlinear trusswork of discrete fibers, coupled with a solid matrix. Numerous studies have utilized a combination of solid elements to model the tissue in focus and structural elements to describe, amongst other things, adjacent tissues, boundary conditions, implants, and medical devices [**?**]. However, there is a scarcity of examples, especially in relation to soft tissue biomechanics, where the underlying material architecture has been explicitly described using conforming structural elements in addition to a solid mesh, each sharing the same degrees of freedom. Curiously, this technique was an early strategy adopted in the modeling of steel rebars within concrete structures [**?**], which, barring a few exceptions, such as a recent study on seismic applications [**?**], has since been abandoned because of its inability to characterize cracking and slipping. Concerning biomechanical applications, truss elements representing active muscle fibers and solid elements describing a nonlinear viscoelastic continuum were combined in the Superpositioned Muscle Finite Element model to capture both active and passive muscle behavior [**?**]. In another study, collagen fibers were modeled using a Voronoi-based network within a neo-Hookean matrix to investigate fiber-matrix interaction during uniaxial loading [**?**]. Along similar lines, discrete 1D fibers were modeled as flexural beams running along the edges of amorphous tetrahedral solid elements [**?**]. A somewhat different approach integrated Timoshenko beam elements and a hyperelastic matrix through a mortar-based method, thereby eliminating the need for conforming meshes at the fiber-matrix interface [**?**].

Within this broader context, the characteristic organization of the cornea is distinctive, as the entire load-bearing capacity of the tissue is entrusted to the collagen fibril skeleton, which forms a true microstructural scaffold. The presented model, therefore, represents a substantial departure from the aforementioned approaches, which simply embed fibers within the extracellular matrix, typically address the presence of the fibers only in a local sense, and importantly, do not portray constituent fibers as a complex mechanically autonomous structure. The application of this modeling strategy to the human cornea could provide new insights concerning the relevance of

the structural organization on physiological and pathological tissue behaviors, since the progressive loss of stiffness can be attributed to the failure of individual components within the reinforcing microstructure. Similarly, a key advantage is its ability to characterize how different components relate to each other spatially and how this relationship changes with and contributes to the development of disease, for instance, the relative shearing of adjacent collagen lamellae due to a reduction in the density and/or mechanical integrity of crosslinks.

Clearly, a new modeling approach necessitated a revisitation of the material parameters, which have been calibrated to experimental ex vivo data taken from the literature, as well as informed by our past modeling endeavors. An in-depth analysis concerning the effect of the cornea's geometric discretization was also carried out, revealing an inherent mesh-dependency of the model arising from the intra-laminar and inter-laminar crosslinks that form a unit cell. However, most significantly, we have shown that the proposed model, whilst using relatively simplistic numerical methods, albeit in a novel and innovative way, is sufficiently advanced for describing corneal pathologies such as ectasia and keratoconus. By applying a spatial reduction in the stiffness of all tissue constituents, it was possible to simulate localized mechanical instability leading to the formation of a conus to an extent that more closely resembles clinical observations compared to previously reported approaches. Surprisingly, we were also able to obtain favorable results for the variance-based model when applied to the simulation of keratoconus in the cornea, predicting a satisfactory shape for the conus. This can be explained by the fact that, with the support of the couple multiscale model, we have found constitutive parameters somewhat different from those used in previous studies, cf. [**?**]. Specifically, the proportions of the various mechanical contributions shifted towards a heightened stiffness of the collagen fibrils relative to the isotropic ECM material, following the indications obtained from the coupled multiscale model.

The conception of the presented multiscale model was motivated by our long-term goal of effectively modeling the evolution of the keratoconic cornea, which cannot be accurately simulated using traditional continuum models. Specifically, purely continuum models cannot replicate the degree of thinning and the variability in thickness at different locations of the cornea [**?**]. However, whilst demonstrating a clear improvement in this regard, the model is still unable to suitably capture the thinning of the cornea (50% based on clinical observations) to the extent that the trusswork alone is able to characterize [**?**]. It is evident that the progressive degeneration of the microstructure alone does not fully encapsulate keratoconus; it is likely that the deterioration in the content and organization of the corneal stroma is associated with a loss in fluid content, leading to a reduction in volume and therefore thinning. In view of this, enforcement of the incompressibility constraint is not necessarily applicable to the tissue in its diseased state, and a biphasic model of the solid extracellular matrix, currently under development, would be more appropriate in characterizing such phenomena. This work, therefore, represents a fundamental first step, and going forward, the coupling of an explicit microstructure and a poroelastic description of the ECM will be instrumental in modeling the thinning of the cornea in localised regions and in reproducing, according to the specific patient, the actual geometry of the pathology.

There are certain limitations associated with the current model and its implementation. For one, whilst the number of degrees of freedom is unchanged compared to conventional continuum approaches, the large number of truss and solid elements for even moderately discretized geometries can lead to significant computational expense and lengthy simulation times. However, this issue is partially mitigated through concurrent computing, as by using the dynamic relaxation solver, each element is managed independently of the others. Another shortcoming is that the model does not consider the biological and chemical aspects associated with keratoconus and other diseases, such as endothelial dysregulation and corneal swelling. A factor that would be remedied with the inclusion of the previously mentioned biphasic description of the ECM. Lastly, as has already been alluded to, the mathematical portrayal of the microstructure is generalized, representing only a fraction of the lamellae present in the real cornea. Computational limitations at the present time make it infeasible to model the entire collagenous architecture of the cornea in the manner presented here. The behavior of a multilayered trusswork was recently investigated for an increasing number of laminar layers, leading to the definition of a continuum equivalent anisotropic material [**?**]. Future strategies may also rely on the advent of sophisticated physics-based machine learning techniques to model the lamellar structure and effectively bridge different length-scales.

Finally, the need for patient-specific material properties represents an ongoing challenge if the effective numerical modeling of the cornea for various clinical and research-based applications is to be fully realized, a factor that depends greatly upon the availability of data garnered from in vivo testing methods, which at the present time remains a bottleneck in the modeling of not just the cornea, but all load-bearing soft biological tissues.

Acknowledgements

This work was supported by the Italian Ministry of University and Research (MUR) under the PRIN 2022 project CORTIS (Grant No. 2022TWKA72). AP and MLDB are grateful for the support of the Italian National Group of Physics-Mathematics (GNFM) belonging to the Italian National Institution of High Mathematics "Francesco Severi" (INDAM).

Appendix A Truss Element Tangent Stiffness Matrix Derivation

The derivation of the tangent stiffness matrix relating to a nonlinear large deformation truss element, first introduced during the discussion of the formulation in Section (**??**), is a modified form of that presented in [**?**]. To begin with, the directional derivative of the current length vector, $l\mathbf{n} = (\mathbf{x}_b - \mathbf{x}_a)$, is determined as

$$D\left[\mathbf{x}_b - \mathbf{x}_a\right]\left[\mathbf{u}\right] = \left.\frac{d}{d\epsilon}\right|_{\epsilon=0} \left(\mathbf{x}_b + \epsilon\mathbf{u}_b - \mathbf{x}_a - \epsilon\mathbf{u}_a\right) = \left(\mathbf{u}_b - \mathbf{u}_a\right),$$

which is based on the definitions of the scalar length of the truss, $l = \{(\mathbf{x}_b - \mathbf{x}_a) \cdot (\mathbf{x}_b - \mathbf{x}_a)\}^{1/2}$, and the unit vector, $\mathbf{n} = (\mathbf{x}_b - \mathbf{x}_a)/l$, describing its direction in space. We can then determine the directional derivatives of several quantities required for the subsequent derivation, such as,

$$D\left[l^{-1}(\mathbf{x})\right][\mathbf{u}] = -l^{-2}\mathbf{n} \cdot (\mathbf{u}_b - \mathbf{u}_a)\,,$$

$$D\left[\lambda(\mathbf{x})\right][\mathbf{u}] = \frac{1}{L}\mathbf{n} \cdot (\mathbf{u}_b - \mathbf{u}_a)\,,$$

where, $\lambda = l/L$, is the non-dimensional stretch of the deformed truss. The directional derivative of the truss's internal force at Node b with respect to the elements displacement, $\mathbf{u} = [\mathbf{u}_\mathrm{a}, \mathbf{u}_\mathrm{b}]^T$, following on from the nodal internal force definitions in Eq. (**??**), and the application of the aforementioned expressions, is then derived as

$$\begin{aligned}
&D\left[\mathbf{T}_b(\lambda(\mathbf{x}), \mathbf{n}(\mathbf{x}))\right][\mathbf{u}] \\
&= D\left[P(\lambda(\mathbf{x}))\right][\mathbf{u}]A\mathbf{n} + P(\lambda)D\left[A\mathbf{n}(\mathbf{x})\right][\mathbf{u}] \\
&= \frac{dP(\lambda)}{d\lambda}D\left[\lambda(\mathbf{x})\right][\mathbf{u}]A\mathbf{n}(\mathbf{x}) + P(\lambda)A\left(D\left[l^{-1}(\mathbf{x})\right][\mathbf{u}](\mathbf{x}_b - \mathbf{x}_a) + \frac{1}{l}D\left[\mathbf{x}_b - \mathbf{x}_a\right][\mathbf{u}]\right) \\
&= \frac{\mathcal{A}(\lambda)A}{L}\mathbf{n} \cdot (\mathbf{u}_b - \mathbf{u}_a)\mathbf{n} + P(\lambda)AlD\left[l^{-1}(\mathbf{x})\right][\mathbf{u}]\mathbf{n} + \frac{P(\lambda)A}{l}\left(\mathbf{u}_b - \mathbf{u}_a\right) \\
&= \frac{\mathcal{A}(\lambda)A}{L}\mathbf{n} \cdot (\mathbf{u}_b - \mathbf{u}_a)\mathbf{n} - \frac{P(\lambda)A}{l}\mathbf{n} \cdot (\mathbf{u}_b - \mathbf{u}_a)\mathbf{n} + \frac{P(\lambda)A}{l}\left(\mathbf{u}_b - \mathbf{u}_a\right) \\
&= \left(\frac{\mathcal{A}(\lambda)A}{L} - \frac{P(\lambda)A}{l}\right)(\mathbf{n} \otimes \mathbf{n})\left(\mathbf{u}_b - \mathbf{u}_a\right) + \frac{P(\lambda)A}{l}(\mathbf{u}_b - \mathbf{u}_a) \\
&= [\alpha(\lambda) - \beta(\lambda)](\mathbf{n} \otimes \mathbf{n})\left(\mathbf{u}_b - \mathbf{u}_a\right) + \beta(\lambda)\mathbf{I}\left(\mathbf{u}_b - \mathbf{u}_a\right)\,,
\end{aligned}$$

which, given that, $D\left[\mathbf{T}_a(\mathbf{x})\right][\mathbf{u}] = -D\left[\mathbf{T}_b(\mathbf{x})\right][\mathbf{u}]$, due to Eq. (**??**), gives rise to the matrix representation of the element tangent stiffness matrix detailed in Eq. (**??**) with the individual contributions provided in Eq. (**??**).

Appendix B Variance-based continuum model of corneal tissue

A brief overview of the key aspects relating to the variance-based model is provided here; however, for a more expansive detailing, the reader is referred to [**?**]. The model consists of two families of spatially dispersed collagen fibrils, such that the cornea is represented as a reinforced anisotropic material, where the specific orientation of

fibrils follows the most advanced findings in the literature [**?**]. The total strain energy consists of three terms

$$\Psi = \Psi_{\text{vol}} + \Psi_{\text{iso}} + \Psi_{\text{aniso}}\,,$$

with Ψ_{vol} denoting the volumetric strain energy, which takes the form

$$\Psi_{\text{vol}}(J) = \frac{1}{4}\,K\,(J^2 - 1 - 2\log J),$$

where $J > 0$ is the determinant of the deformation gradient $\mathbf{F}$, and K a penalization coefficient analogous to the bulk modulus. The isotropic energy Ψ_{iso} follows the Mooney-Rivlin model and is defined as

$$\Psi_{\text{iso}}(\overline{I}_1, \overline{I}_2) = \frac{1}{2}\mu_1(\overline{I}_1 - 3) + \frac{1}{2}\mu_2(\overline{I}_2 - 3)\,, \quad \overline{I}_1 = \operatorname{tr}\overline{\mathbf{C}}\,, \quad \overline{I}_2 = \frac{1}{2}[(\operatorname{tr}\overline{\mathbf{C}})^2 - \operatorname{tr}(\overline{\mathbf{C}}^2)]\,,$$

where $\mu = \mu_1 + \mu_2$ is the elastic shear modulus of the material. The terms $\overline{I}_1$ and $\overline{I}_2$ denote the first and the second invariants, respectively, of the isochoric Cauchy-Green deformation tensor $\overline{\mathbf{C}} = \overline{\mathbf{F}}^T\overline{\mathbf{F}}$, with $\overline{\mathbf{F}} = J^{-1/3}\mathbf{F}$. The anisotropic strain energy Ψ_{aniso} describing the contribution of the two collagen fibril families is

$$\Psi_{\text{aniso}}(\overline{I}^*_{4M}, \sigma^2_{I_4 M}) = \sum_{M=1}^{2} \frac{k_{1M}}{2k_{2M}} \exp\left[k_{2M}\left(\overline{I}^*_{4M} - 1\right)^2\right]\left(1 + K^*_M(\overline{I}^*_{4M})\sigma^2_{I_4 M}\right),$$

where k_{1M} is a stiffness parameter, controlling the fibril behavior at moderate deformations, and k_{2M} is a dimensionless rigidity parameter, regulating the response at large deformations. The pseudo-invariants $\overline{I}^*_{4M}$ are defined as

$$\overline{I}^*_{4M} = \mathbf{H}_M : \overline{\mathbf{C}}\,, \quad \mathbf{H}_M = \langle \mathbf{A}_M \otimes \mathbf{A}_M \rangle = \kappa_M \mathbf{I} + (1 - 3\kappa_M)\mathbf{A}_{M0}\,, \quad \mathbf{A}_M = \mathbf{a}_M \otimes \mathbf{a}_M\,,$$

where $\langle \bullet \rangle$ denotes the average over the unit sphere, $\mathbf{A}_{M0} = \mathbf{a}_0 \otimes \mathbf{a}_0$ refers to the main orientation of the fibril distribution, and the scalar parameter κ_M is defined according to

$$\kappa_M = \frac{1}{4}\int_0^\pi \rho_M(\Theta)\sin^3\Theta d\Theta\,,$$

where $\rho_M(\Theta)$ is the spatial probability distribution (e.g., von Mises). Finally, the relations

$$\sigma^2_{I_4 M} = \overline{\mathbf{C}} : \langle \mathbf{A}_M \otimes \mathbf{A}_M \rangle : \overline{\mathbf{C}} - \left(\mathbf{H}_M : \overline{\mathbf{C}}\right)^2, \quad K^*_M(\overline{I}^*_{4M}) = k_{2M} + 2\,k^2_{2M}\,\left(\overline{I}^*_{4M} - 1\right)^2$$

provide the variance contribution to Ψ_{aniso} and its amplification coefficient, respectively.

References

[] Mishima, S., Hedbys, B.O.: Physiology of the cornea. International ophthalmology clinics **8**(3), 527–560 (1968)

[] Bron, A.J.: The architecture of the corneal stroma. British Journal of Ophthalmology **85**, 379–383 (2001)

[] Maurice, D.M.: The structure and transparency of the cornea. The Journal of physiology **136**(2), 263 (1957)

[] Abahussin, M., Hayes, S., Cartwright, N.E.K., Kamma-Lorger, C.S., Khan, Y., Marshall, J., Meek, K.M.: 3D collagen orientation study of the human cornea using X-ray diffraction and femtosecond laser technology. Investigative Ophthalmology & Visual Science **50**(11), 5159–5164 (2009) https://doi.org/10.1167/iovs.09-3669

[] Meek, K.M., Blamires, T., Elliot, G.F., Gyi, T.J., Nave, C.: The organization of collagen fibrils in the human corneal stroma: a synchroton x-ray diffraction study. Current Eye Research **6**, 841–846 (1987)

[] Aghamohammadzadeh, H., Newton, R.H., Meek, K.M.: X-ray scattering used to map the preferred collagen orientation in the human cornea and limbus. Structure **12**(2), 249–256 (2004)

[] Rabinowitz, Y.S.: Keratoconus. Survey of Ophthalmology **42**, 297–319 (1998)

[] Santodomingo-Rubido, J., Carracedo, G., Suzaki, A., Villa-Collar, C., Vincent, S.J., S., W.J.: Keratoconus: An updated review. Contact Lens and Anterior Eye **45**(3), 101559 (2022) https://doi.org/10.1016/j.clae.2021.101559

[] Simonini, I., Ni Annaidh, A., Pandolfi, A.: Numerical estimation of stress and refractive power maps in healthy and keratoconus eyes. Journal of the Mechanical Behavior of Biomedical Materials **131**, 105252 (2022)

[] Ariza-Gracia, M.A., Zurita, J.F., Piñero, D.P., Rodriguez-Matas, J.F., Calvo, B.: Coupled biomechanical response of the cornea assessed by non-contact tonometry. A simulation study. PLoS ONE **10**(3), 0121486 (2015)

[] Simonini, I., Pandolfi, A.: The influence of intraocular pressure and air jet pressure on corneal contactless tonometry tests. Journal of the Mechanical Behavior of Medical Biomaterials **58**, 75–89 (2016) https://doi.org/10.1016/j.jmbbm.2015.07.030

[] Redaelli, E., Calvo, B., Rodriguez Matas, J.F., Luraghi, G., Grasa, J.: Non-contact tonometry: predicting intraocular pressure using a material—corneal

thickness—independent methodology. Frontiers in Bioengineering and Biotechnology **Volume 12 - 2024** (2024) https://doi.org/10.3389/fbioe.2024.1406870

Studer, H.P., Riedwyl, H., Amstutz, C.A., Hanson, J.V.M., Büchler, P.: Patient-specific finite-element simulation of the human cornea: A clinical validation study on cataract surgery. Journal of Biomechanics **46**(4), 751–758 (2013) https://doi.org/10.1016/j.jbiomech.2012.11.018

Ariza-Gracia, M., Ortillés, , Cristóbal, J., Rodriguez-Matas, J.F., Calvo, B.: A numerical-experimental protocol to characterize corneal tissue with an application to predict astigmatic keratotomy surgery. Journal of the Mechanical Behavior of Biomedical Materials **74**, 304–314 (2017) https://doi.org/10.1016/j.jmbbm.2017.06.017

Montanino, A., Overbeeke, S., Pandolfi, A.: Modeling the biomechanics of laser corneal refractive surgery. Journal of the Mechanical Behavior of Biomedical Materials **145**, 105998 (2023)

Pandolfi, A., Manganiello, F.: A material model for the human cornea. constitutive behavior and numerical analysis. Biomechanics and Modelling in Mechanobiology **5**, 237–246 (2006)

Fantaci, B., Calvo, B., Rodriguez Matas, J.F.: Modeling biological growth of human keratoconus: On the effect of tissue degradation, location and size. Computers in Biology and Medicine **180**, 108976 (2024) https://doi.org/10.1016/j.compbiomed.2024.108976

Falgayrettes, N., Patoor, E., Cleymand, F., Zevering, Y., Perone, J.M.: Biomechanics of keratoconus: Two numerical studies. PLOS ONE **18**(2), 1–25 (2023) https://doi.org/10.1371/journal.pone.0278455

Studer, H., Larrea, X., Riedwyl, H., Büchler, P.: Biomechanical model of human cornea based on stromal microstructure. Journal of Biomechanics **43**(5), 836–842 (2010) https://doi.org/10.1016/j.jbiomech.2009.11.021

Whitford, C., Studer, H., Boote, C., Meek, K.M., Elsheikh, A.: Biomechanical model of the human cornea: Considering shear stiffness and regional variation of collagen anisotropy and density. Journal of the Mechanical Behavior of Medical Biomaterials **42**, 76–87 (2015) https://doi.org/10.1016/j.jmbbm.2014.11.006

Nambiar, M., Seiler, T.G., Büchler, P.: Depth-dependent, experimental characterization of the human corneal stroma. Investigative Ophthalmology & Visual Science **64**(8), 1685–1685 (2023)

Pandolfi, A., Vasta, M.: Fiber distributed hyperelastic modeling of biological tissues. Mechanics of Materials **44**, 151–162 (2012)

[] Miller, C., Gasser, T.C.: A microstructurally motivated constitutive description of collagenous soft biological tissue towards the description of their non-linear and time-dependent properties. Journal of the Mechanics and Physics of Solids **154**, 104500 (2021) https://doi.org/10.1016/j.jmps.2021.104500

[] Miller, C., Gasser, T.C.: A bottom-up approach to model collagen fiber damage and failure in soft biological tissues. Journal of the Mechanics and Physics of Solids **169**, 105086 (2022) https://doi.org/10.1016/j.jmps.2022.105086

[] Pandolfi, A., Gizzi, A., Vasta, M.: A microstructural model of cross-link interaction between collagen fibrils in the human cornea. Philosophical Transactions of the Royal Society A **377**(2144), 20180079 (2019)

[] Pandolfi, A., De Bellis, M.L., Gizzi, A., Vasta, M.: Modeling the degeneration of the collagen architecture in a microstructural model of the human cornea. Mathematics and Mechanics of Solids **28**(1), 196–207 (2023)

[] De Bellis, M.L., Vasta, M., Gizzi, A., Pandolfi, A.: A numerical model of the human cornea accounting for the fiber-distributed collagen microstructure. Mathematics and Mechanics of Solids, 10812865231202024 (2023)

[] Pandolfi, A., De Bellis, M.L.: Continuum versus micromechanical modeling of corneal biomechanics. Mechanics of Materials **199**, 105162 (2024)

[] Simonini, I., Pandolfi, A.: Customized finite element modelling of the human cornea. PloS one **10**(6), 0130426 (2015)

[] Holzapfel, G.A., Gasser, T.C., Ogden, R.W.: A new constitutive framework for arterial wall mechanics and a comparative study of material models. Journal of Elasticity **61**, 1–48 (2000)

[] Simo, J.C., Taylor, R.L.: Quasi-incompressible finite elasticity in principal stretches. continuum basis and numerical algorithms. Computer Methods in Applied Mechanics and Engineering **85**(3), 273–310 (1991) https://doi.org/10.1016/0045-7825(91)90100-K

[] Rivlin, R.S., Saunders, D.W.: Large elastic deformations of isotropic materials. VII. Experiments on the deformation of rubber. Phylosophycal Transactions of The Royal Society of London, A **243** (1951)

[] Bonet, J., Wood, R.D.: Nonlinear Continuum Mechanics for Finite Element Analysis, 2nd edn. Cambridge University Press, Cambridge (2008)

[] Köry, J., Stewart, P.S., Hill, N.A., Luo, X.-Y., Pandolfi, A.: A discrete-to-continuum model for the human cornea with application to keratoconus. Royal Society Open Science **11**(7), 240265 (2024)

[] Belytschko, T., Liu, W.-K., Moran, B., Elkhodary, K.: Nonlinear Finite Elements for Continua and Structures. John Wiley & Sons, New Jersey (2014)

[] Oakley, D.R., Knight Jr, N.F.: Adaptive dynamic relaxation algorithm for non-linear hyperelastic structures part i. formulation. Computer methods in applied mechanics and engineering **126**(1-2), 67–89 (1995)

[] Elsheikh, A.: Finite element modeling of corneal biomechanical behavior. Journal of Refractive Surgery **26**(4), 289–300 (2010)

[] Erdemir, A., McLean, S., Herzog, W., Bogert, A.J.: Model-based estimation of muscle forces exerted during movements. Clinical Biomechanics **22**(2), 131–154 (2007) https://doi.org/10.1016/j.clinbiomech.2006.08.003

[] Phillips, D.V., Zienkiewicz, O.C.: Finite element non-linear analysis of concrete structures. Proceedings of the Institute of Civil Engineering of London **61**(pt 2), 59–88 (1976) https://doi.org/10.1680/iicep.1976.3503

[] Tanaka, S., Hori, M., Ichimura, T.: Hybrid finite element modeling for seismic structural response analysis of a reinforced concrete structure. Journal of earthquake and tsunami **10**(05), 1640015 (2016)

[] Hedenstierna, S., Halldin, P., Brolin, K.: Evaluation of a combination of continuum and truss finite elements in a model of passive and active muscle tissue. Computer Methods in Biomechanics and Biomedical Engineering **11**(6), 627–639 (2008) https://doi.org/10.1080/17474230802312516

[] Lake, S.P., Hadi, M.F., Lai, V.K., Barocas, V.H.: Mechanics of a fiber network within a non-fibrillar matrix: model and comparison with collagen-agarose co-gels. Annals of Biomedical Engineering **40**, 2111–2121 (2012)

[] Zhang, L., Lake, S.P., Barocas, V.H., Shephard, M.S., Picu, R.C.: Cross-linked fiber network embedded in an elastic matrix. Soft Matter **9**(28), 6398–6405 (2013)

[] Kakaletsis, S., Lejeune, E., Rausch, M.: The mechanics of embedded fiber networks. Journal of the Mechanics and Physics of Solids **181**, 105456 (2023) https://doi.org/10.1016/j.jmps.2023.105456